

Seismic stratigraphy and deep-water sedimentary evolution of the southern Mozambique margin: Central Terrace and Mozambique Fracture Zone



Ya Gao^{a,b}, Dorrik Stow^{b,c}, Yong Tang^{b,d,e,*}, Xinong Xie^{a,b,*}, David J.W. Piper^f

^a Hubei Key Laboratory of Marine Geological Resources, China University of Geosciences (CUG), Wuhan 430074, PR China

^b College of Marine Science and Technology, China University of Geosciences (CUG), Wuhan 430074, PR China

^c Institute of Geo-Energy Engineering, Heriot Watt University, Edinburgh EH14 4AS, UK

^d Second Institute of Oceanography, Ministry of Natural Resources (MNR), Hangzhou 310000, PR China

^e Key Laboratory of Submarine Geosciences, Ministry of Natural Resources (MNR), Hangzhou 310000, PR China

^f Natural Resources Canada, Geological Survey of Canada (Atlantic), Bedford Institute of Oceanography, P.O. Box 1006, Dartmouth, Nova Scotia B2Y 4A2, Canada

ARTICLE INFO

Editor: Wilfried Jokat

Keywords:

Southern Mozambique margin
Mozambique Fracture Zone
Downslope-Alongslope deposition
Contourite Depositional System

ABSTRACT

Based upon new seismic reflection data, this study reveals the development of a complex sedimentary system on the lower-slope terrace off Maputo on the southern Mozambique margin. The deep-water sedimentary system clearly shows the interaction of downslope and alongslope processes. Downslope features include: a pronounced canyon, slope creep, submarine slides, and multi-stage mass-transport deposits. Alongslope features include: contourite drifts and sediment waves, erosional moats, valleys, erosive surfaces and a distinctive contourite terrace. We show an evolution through time as follows: (1) restricted marine sedimentation during the Early Cretaceous after the initial break-up, with slope progradational clinoforms and hemipelagite drape developed; (2) open marine sedimentation characterized by the onset of alongslope sedimentary processes during the Late Cretaceous and development of a contourite depositional system; (3) downslope gravity processes dominated sedimentation during the Paleocene-Eocene, including development of a canyon and submarine fan; and (4) an alongslope contourite depositional system was re-established on the lower slope in the Middle Miocene, while turbidites (from a northern source) covered the Mozambique Basin. The Mozambique Fracture Zone marks a distinct and steep slope seaward of the contourite terrace, and has significantly influenced both contourite and turbidite deposition. Our study provides new insights into the onset and evolution of bottom current control on margin sedimentation, the interaction of downslope and alongslope processes and how these processes have jointly sculpted this part of the southern Mozambique margin.

1. Introduction

There are a wide range of processes that operate in deep-water to erode, transport and deposit sediment across the continental margin and on the deep basin floor. These include a variety of gravity-driven (downslope), current-driven (along-slope), pelagic/hemipelagic and chemogenic processes (Rebesco and Camerlenghi, 2008; Mulder et al., 2011; Pickering and Hiscott, 2016; Stow and Smillie, 2020). Each of these individual processes shapes the continental margin in different ways and gives rise to a distinctive deposit or sediment facies.

Whereas much earlier work focused on the role of downslope processes (e.g., turbidity currents, mass transport and sediment failure) in sculpting deep-sea morphology and sedimentation (Mulder et al., 2008; Piper and Normark, 2009; Kneller et al., 2016), more recent studies have demonstrated that bottom currents can be equally significant in

shaping continental margins and their role in this context may have been underestimated (e.g., Stow, 2002; Preu et al., 2012, 2013; Rebesco et al., 2014; Hernández-Molina et al., 2016). Bottom-water circulation can affect sediment distribution by transporting suspended materials or removing previously deposited sediments, and further deposit this material as contourites. Non-deposition/erosion can occur during higher-velocity periods (Stow et al., 2008; Rebesco et al., 2014). With the simultaneous capability to erode, transport and deposit sediments, bottom current processes have thus played a critical role in shaping continental margins through geological time.

This study focuses on the southern Mozambique continental margin (SMCM) southeast of the Mozambique Coastal Plain, which is fed by the Limpopo and Save rivers (Fig. 1). Different from the traditional passive continental margin, with a shelf, slope and rise configuration, the SMCM has an unusual morphology with stepped terraces (see the

* Corresponding authors at: College of Marine Science and Technology, China University of Geosciences (CUG), Wuhan 430074, PR China.

E-mail addresses: tangyong@sio.org.cn (Y. Tang), xnxie@cug.edu.cn (X. Xie).

<https://doi.org/10.1016/j.margeo.2020.106187>

Received 14 December 2019; Received in revised form 22 March 2020; Accepted 26 March 2020

Available online 27 April 2020

0025-3227/ © 2020 Elsevier B.V. All rights reserved.

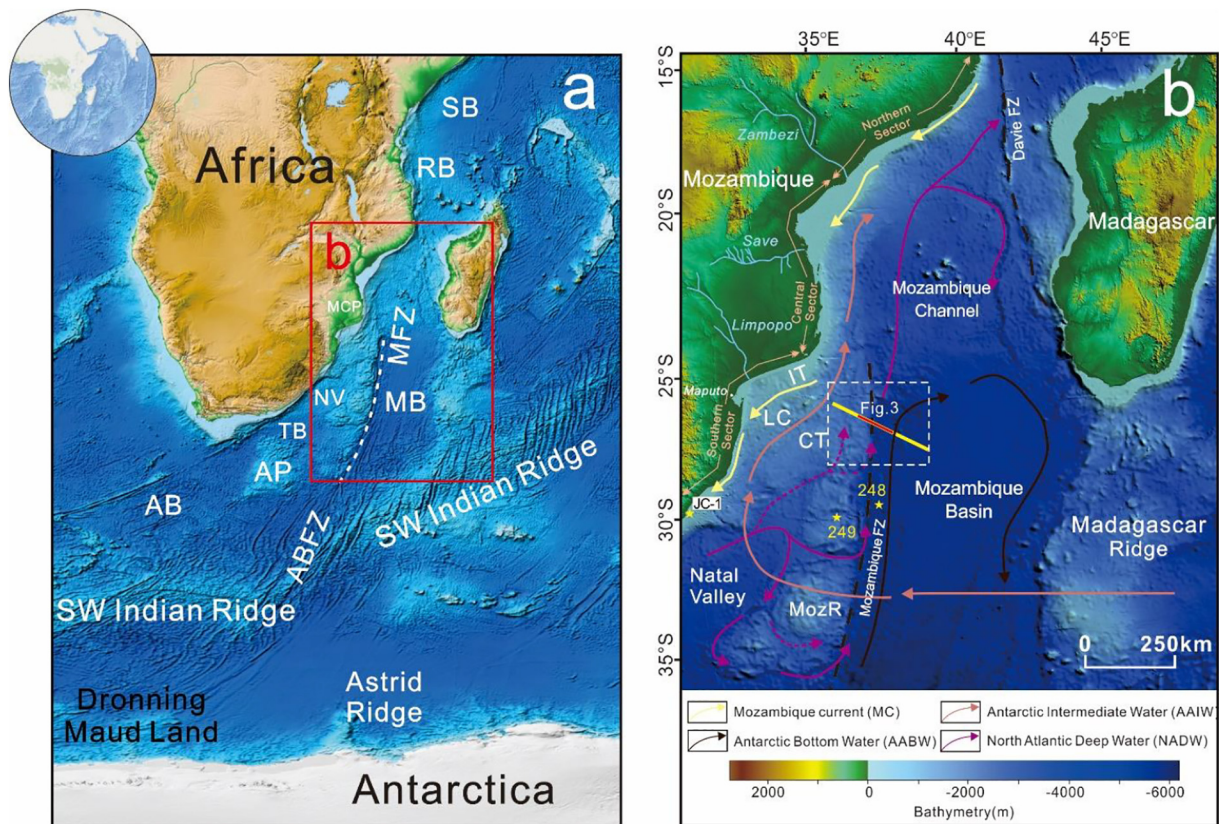


Fig. 1. (a) World location and overview map of the SW Indian Ocean; Abbreviations: SB = Somali Basin; RB = Rovuma Basin; NV = Natal Valley; TB = Transkei Basin; AP = Agulhas Plateau; AB = Agulhas Basin; MCP = Mozambique Coastal Plain; MB = Mozambique Basin; MFZ = Mozambique Fracture Zone; ABFZ = Andrew Bain Fracture Zone; (b) Bathymetric map (extrapolated from the GEBCO gridded bathymetry data) of the Mozambique Channel, showing 1) the whole seismic reflection profile (yellow) crossing from the CT to the MB and the presented part (red) in this study; 2) DSDP drilling sites (stars in yellow) used in the study; 3) fracture zones (dashed lines), modified after König and Jokat (2010); Fischer et al. (2016); Massuanganhe et al. (2018) and 4) schematic position of present-day water masses (Wiles et al., 2014; Thiéblemont et al., 2019). Abbreviations: MoR = Mozambique Ridge; FZ = Fracture Zone; IT = Inharrime Terrace; LC = Limpopo Cone; CT = Central Terrace. (For interpretation of the references to colour in this figure legend, the reader is referred to the web version of this article.)

morpho-sedimentary map shown by Thiéblemont et al., 2019). The terraces extend to the Mozambique Basin (MB) towards the southeast, dropping from about 2000 m to between 3000 and 6000 m crossing the Mozambique Fracture Zone (MFZ), with the absence of a continental rise. This part of margin is contiguous with the Mozambique Ridge (MozR, Fig. 1a, b) to the south, which together forms a complex topography that interacts with a variety of water masses. Although recent papers have reported the existence of a contourite depositional system (CDS) in this region (e.g. Uenzelmann-Neben, 2002; Fischer and Uenzelmann-Neben, 2018; Thiéblemont et al., 2019), the deep-water depositional evolution locally in the SMCM, and especially the role of bottom currents in the construction of this continental margin, is still poorly known.

As a contribution towards better understanding this margin, here we present a seismostratigraphic analysis of the lower part of the southern Mozambique continental slope, comprising a submarine terrace, named the Central Terrace (CT), and the adjacent part of the MB. The main objective of this work is to determine the timing of onset and subsequent evolution of the bottom current control on margin sedimentation, and also consider the interaction of downslope and upslope processes in shaping the margin morphology by identifying sedimentary features in a series of evolutionary stages. Furthermore, we evaluate the possible role of the MFZ and the origin of the associated escarpment.

2. Regional setting

2.1. Tectonic and geological background

The Mozambique Channel is located in the southwest Indian Ocean, between the coast of East Africa and Madagascar (Fig. 1a). It opened from the north and then gradually extended southward during the break-up processes of supercontinent Gondwana (Jokat et al., 2003; Eagles and König, 2008; Leinweber and Jokat, 2012; Mueller and Jokat, 2017; 2019). The initial rifting dates back to Early-Middle Jurassic, as Mueller and Jokat (2017) identified the oldest oceanic crust near the northern sector of Mozambique (Fig. 1b), indicating the opening of the northern Mozambique Basin (Reeves, 2000; Leinweber and Jokat, 2012). The next stage is characterized by a significant change of the spreading direction from SE to SSW, during which the Davie Fracture Zone (DFZ) formed, and rifting continued southward to the central sector (Mueller and Jokat, 2019; Vormann et al., 2020; Fig. 1b), with the opening of the central Mozambique Basin. In the southern sector, the Natal Valley and Mozambique Ridge (MozR; Fig. 1a and b) are considered to have formed until the Early Cretaceous (e.g., König and Jokat, 2010; Leinweber and Jokat, 2012; Hanyu et al., 2017; Jacques et al., 2019; Mueller and Jokat, 2019).

At present, the offshore continuation of the Mozambique Coastal Plain (MCP in Fig. 1a) is characterized by a stepped terrace-like morphology: the Inharrime Terrace located at ~300 m water depth; the Limpopo Cone built up by Limpopo river sediments under current restriction (Martin, 1981) at 800–1500 m; and the Central Terrace at

~2000 m (Martin et al., 1982; Preu et al., 2011; Thiéblemont et al., 2019). The CT and MozR together are bounded by a N-S trending escarpment along the eastern margin (Fig. 1b; König and Jokat, 2010; Mueller and Jokat, 2019). Compared to the better known northern-central Mozambique margin (e.g., the crustal structure and associated continent-ocean boundary (Mueller et al., 2016; Senkans et al., 2019; Vormann et al., 2020), it is worth noting that the crustal nature of this part (i.e., from IT to CT) is still unclear. Recent work favours a continental origin (Hanyu et al., 2017; Mueller and Jokat, 2019). In this study, we have followed the general identification of the margin as the offshore area from the coastal zone across the shelf and terraced slope configuration, as also followed by Thiéblemont et al. (2019) and Preu et al. (2011).

Regional stratigraphy indicates that the deposition off the southern Mozambique margin started no later than the Early Cretaceous (Lawver et al., 1992; Veevers, 2012), which is confirmed by drilling results (Martin et al., 1982). The J(c)-I bore-hole located on the continental shelf 24 km east of the Natal coast and the Deep Sea Drilling Project (DSDP) Site 249 on the northern MozR both encountered Early Cretaceous basement (Fig. 1b; Du Toit and Leith, 1974; Simpson et al., 1974). Thereafter, during regional transgression, a deep-water sedimentary environment gradually developed.

2.2. Stratigraphic framework

In the drifting stage, only the broad stratigraphic outlines of the region are known, based mainly on extrapolation of studies from the better known South African margin: Du Toit and Leith (1974) identified the sedimentary gaps in the J(c)-1 core based on biostratigraphy; DSDP 249 was dated based on biostratigraphic age determinations (Simpson et al., 1974); Dingle et al. (1978) picked the key reflectors from seismic lines and assigned the age range by correlating it to the sedimentary hiatus in the JC-1 borehole (Du Toit and Leith, 1974) and with DSDP 249 (Simpson et al., 1974); Preu et al. (2011) identified four major sedimentary sequences of the Inharrime Terrace based on structural discontinuities, and further correlated the bounding surfaces to the seismic stratigraphy provided by Dingle et al. (1978) and Martin (1981); Fischer et al. (2016) and Fischer and Uenzelmann-Neben (2018) divided the sedimentary units on seismic profiles and made age assignment based on correlation with DSDP 249 (Simpson et al., 1974). These studies lead to the identification of four regional reflecting horizons (termed McDuff, Angus, Jimmy, L), all of which represent significant unconformities and/or facies changes. The McDuff horizon was defined as marking the Cenomanian-Turonian boundary (Dingle et al., 1978). Although it cannot be equated directly to the sediment packages of the MozR because of the different geological background, the hiatus between Cenomanian and Turonian was also identified in DSDP 249 (Simpson et al., 1974). Reflector Angus was considered to be a structural discontinuity linked to the mid-Cenozoic hiatus (Dingle et al., 1978), which correlates well with the basal Oligocene hiatus in the JC-1 borehole and can be equated with the Maastrichtian-Lower Miocene hiatus in DSDP 249 (Martin et al., 1982). A reflector within the Angus-Jimmy sequence has been assigned an age of Early Miocene, based on which Martin (1981) dated reflector Jimmy as post-Early Miocene. The pre-Angus sequence is widely distributed in the SMCM, Pliocene-Holocene deposition accumulated within the area of Limpopo Cone and the Inharrime Terrace, while on the CT post-Angus sediments are either absent or reworked and thin (Martin et al., 1982), indicating that depocenters shifted after horizon Angus times. In this way, the discontinuity L described by Martin (1981) can be traced only within the Inharrime Terrace and the southern Limpopo cone regions (Preu et al., 2011), without borehole correlation and age assignments.

Schlich (1974) described the sedimentary sequence of the Mozambique Basin in the DSDP 248 well data analysis report: the total penetration reached 434 m including 12 m of basalt, three sedimentary units and their bounding unconformities were identified; the lowermost

unit III comprises pelagic sediments of late Paleocene age, overlying the basalt that forms the oceanic basement of 72 ± 7 Ma confirmed through K–Ar dating; the overlying depositional unit II consists of volcanic silty clay and silt-sized grains with an Eocene age, which has a marked lithological contrast to the brown clay of unit III; at the top of this unit, a distinct stratigraphic hiatus from late Eocene to early-middle Miocene was recognized; the overlying two units were mostly deposited below the regional carbonate compensation depth; the lithology in topmost unit I is mainly silts, clays, and coarse sands and the deposition after the middle Miocene shows a strong terrigenous influence with coarse-grained turbidites that derived from the East African continent and/or Madagascar reaching this part of the basin.

2.3. Oceanographic setting

At present, the oceanic circulation within the Mozambique Channel of the Indian Ocean as part of Agulhas Current system is quite complicated (Lutjeharms, 2006). It mainly comprises two systems of Mozambique Current and Mozambique undercurrent that flow in the opposing directions (De Ruijter et al., 2002; Quartly et al., 2013). Southward-flowing Mozambique currents are anticyclonic eddy-dominated western boundary currents (DiMarco et al., 2002; Schouten et al., 2003; Preu et al., 2011). They carry upper layers of Tropical Surface Water (TSW) and Subtropical Surface Water (STSW) flowing at < 200 m (Ullgren et al., 2012), a middle layer of South Indian Central Water (SICW) occupying a permanent thermocline at 200–600 m (Fig. 2c), and a lower layer of the Red Sea Water (RSW) between 900 and 1200 m (Quadfasel, 2001).

Northward-flowing Mozambique undercurrents consist of three major water masses: Antarctic Intermediate Water (AAIW), North Atlantic Deep Water (NADW) and Antarctic Bottom Water (AABW) (Fig. 2b). At water depths between 800 and 1500 m, the AAIW crosses westward over the Madagascar ridge, entering the MB and flowing along the Mozambican continental slope (Figs. 1b and 2c). The NADW at between 2200 and 3500 m flows into the southern Mozambique Basin (sMB) via Natal Valley (Fig. 1b; Toole and Warren, 1993; van Aken et al., 2004), close to the study area. Decreasing water depths (northern boundary of the Natal Valley and western boundary of the MozR) form topographic barriers so that the NADW is forced to split into several water masses with different pathways (Fig. 1b). The upper volume of the NADW continues its northward flow across the southern Mozambican continental slope while the remaining NADW forms a return current and flows along the MozR (van Aken et al., 2004; Wiles et al., 2014; Fischer and Uenzelmann-Neben, 2018), which may create relatively complex pathways locally (Fig. 1b) and is of special interest to this study. A similar situation also occurs in the Mozambique Channel, where parts of the NADW enter into the Somali Basin and the rest acts as a southerly return current (van Aken et al., 2004; Ullgren et al., 2012; Fig. 1a). The underlying AABW spreading from the Agulhas Basin is restricted to below 4000 m (Fig. 2c). It is constrained by the basin depth, which blocks its passage towards the north, so it flows back southwards along the eastern boundary of the MB (Kolla et al., 1976, 1980). Both the deep part of the NADW and the AABW have a very low temperature and relatively low salinity (Fig. 2b). The interfaces between these two water masses are located respectively at 1500–2200 m and 3500–4000 m.

3. Material and methods

The seismic data used for the objectives outlined above were provided by the Second Institute of Oceanography, using the scientific research vessel *Xiangyanghong No.10* for data acquisition in 2016. The multi-channel 2D airgun reflection seismic reflection profile is 360 km long. For this study only 127 km are interpreted (Fig. 1b). A Sercel GII-Gun with a volume of 1340 cu inch operated at 2000 psi was used as seismic source and towed at 10 m depth, working at a shot interval of

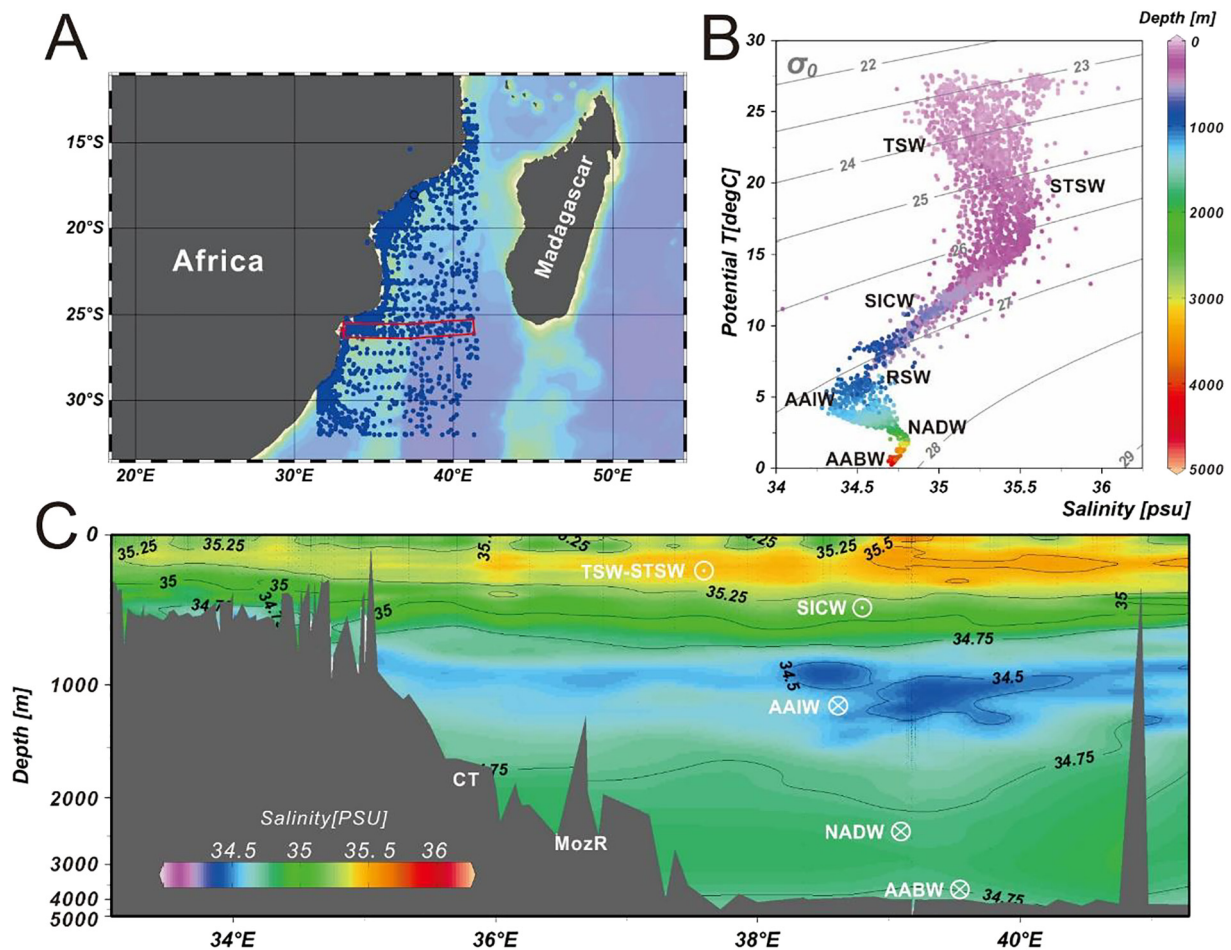


Fig. 2. (a) Base map with the CTD data distribution of the Mozambique Channel; the red box represents the CTD sites (World Ocean Database, 2013) used for (b) Potential temperature vs. Salinity diagram of the representative temperature - depth section (World Ocean Database, 2013) and (c) Salinity section showing the distribution of the main water masses present in the study area (World Ocean Database, 2013). Abbreviations: TSW = Tropical Surface Water; STSW = Sub-Tropical Surface Water; SICSW = South Indian Central Water; RSW: Red Sea Water; AAIW = Antarctic Intermediate Water; NADW = North Atlantic Deep Water; AABW = Antarctic Bottom Water. Referred from Miramontes et al. (2019) and Thiéblemont et al. (2019). (For interpretation of the references to colour in this figure legend, the reader is referred to the web version of this article.)

50 m. The recording length was 14 s two-way travel time (TWT) and the sampling rate was set at 2 ms. The streamer is approximately 1475 m with 108 channels and Common Depth Point (CDP) sorting with a CDP spacing of 12.5 m. Standard seismic processing was provided by China National Offshore Oil Corporation, including de-noising, amplitude compensation, energy equalization of gun offset, surface related multiple elimination, common reflection surface stack, frequency division attenuated diffraction multiple times, post-stack time migration. The profile was converted to depth of the present-day seafloor using an average velocity of 1500 m/s for the water column.

In order to show a better regional overview and reveal the general stratigraphic situation for correlation in the study area, the following databases were used: 1) The General Bathymetric Chart of the Oceans (GEBCO), from which the bathythermograph data were extracted, and then these gridded bathymetry data were viewed and further processed using Global Mapper 18.0 software. 2) Deep Sea Drilling Project Reports and Publications, where the initial reports of Site 249 and Site 248 are provided. 3) The World Ocean Database 2018 (Boyer et al., 2019), where oceanographic data are obtained and further visualisation by Ocean Data View 4.5.3 software.

Seismic units and their boundaries are defined by the occurrence of seismic features such as truncation, onlap, hiatus and distinct surfaces associated with facies change (Table 1). These seismic sections and boundaries were subsequently correlated to previous regional seismic

stratigraphy studies for age assignments (Table 2). To constrain the multiple possibilities when confirming the sedimentary facies interpreted on just one seismic profile, some of the seismic facies are discussed based on the correlations to the established diagnostic criteria, published study cases, with the associated regional geological background.

4. Results

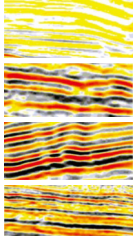
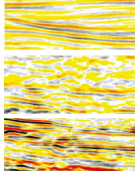
4.1. Seismic stratigraphic framework

The seismic profile extends from the CT at ~2000 m depth across the MFZ to the MB at ~3000 m depth. Seismic units and boundaries are presented within three regions (Fig. 3). Regional unconformities are identified and sedimentary units are named from bottom to top (Figs. 4 and 6). Because direct correlation across the MFZ is not possible (Fig. 5), units and unconformities are given different designations on the CT and in the MB, the top of basement reflections are termed Tg and tg, respectively.

4.1.1. Mozambique Central Terrace

Three regional unconformities within the CT are identified and named as T1, T2 and T3 from top to bottom. T3 is marked by downlapping reflection pattern of overlying strata (Fig. 4, CDPs 15409-18809

Table 1
(a) Seismic facies in the units of CT area. (b) Seismic facies in the units of the MB.

Sequence	Internal reflection pattern	Frequency	Amplitude	Continuity	Typical case
(a)					
Unit 4A	Subparallel, locally chaotic	Low-Moderate	Weak	Intermediate, locally discontinuous	
Unit 3A	Parallel-subparallel	Moderate-high	Moderate-strong	High-intermediate locally discontinuous	
Unit 2	Subparallel, locally wave	Mostly high	Strong-moderate	Intermediate-high	
Unit 1	Parallel-subparallel	Low-moderate	Weak-moderate	High	
(b)					
Unit 3b	Parallel-subparallel locally wave	Moderate-high	Moderate	High-intermediate, locally discontinuous	
Unit 2b	Subparallel, locally chaotic	High-moderate, locally low	Weak-moderate	Intermediate, largely discontinuous	
Unit 1b	Subparallel, locally chaotic	Low-moderate	Weak-moderate	Low, locally continuous	

in unit 2A) and also marks the boundary between different sediment accumulation patterns. Most of T2 shows a truncation reflection pattern, and T1 is distinguished by a radical change in seismic facies. Locally T1 truncates underlying strata and has onlapping of overlying strata as well (Fig. 4, CDPs 14609–16209 in unit 3A).

Seismic unit 1 is composed of subunits 1A and 1B. The lower subunit 1A is characterized by a set of continuous, parallel-subparallel, weak-moderate reflectors with isolated stronger amplitude or low frequency reflectors in an aggradational stacking pattern. It overlies a slightly faulted basement. Towards the southeast the reflectors slope downward and show slightly lower frequency (Fig. 4, CDPs 19009–20609 at 4.7–5.5 s TWT). Unit 1B contains moderate frequency and amplitude reflectors at its base, which are overlain by mostly continuous reflectors of much higher frequency and amplitude. Its top boundary contains channel-like incisions, under which the continuous reflectors are locally interrupted and become irregular, making them hard to trace (Fig. 4, CDPs 18659–19109 at 4.6 s TWT). In the southeast, downlap reflection can be observed at the base of the unit, resulting in a prograding reflection stacking pattern (Fig. 4, CDPs 19409–20,209 at 5.0 s TWT). The total thickness of unit 1A and 1B varies, ranging from 0.5 to 0.8 s TWT with a maximum in the middle part of the CT. The oblique prograding stacking pattern represents a sequence of clinoforms.

Seismic unit 2 is divided into subunits 2A and 2B by a boundary that may represent a change in sedimentary setting. This unit is on average 1.2 s TWT thick. Unit 2A consists of sub-parallel, moderate amplitude, mostly high frequency, generally continuous reflectors, which are slightly cut around CDPs ~17209. Wavy reflection patterns with lower frequency and amplitude reflectors can be identified (Fig. 4, CDPs 17209–19209 in unit 2A), linking to a series of low-moderate frequency and amplitude, mostly high continuity, inclined reflectors (Fig. 4, CDPs 19209–21009 at 4.3–5.1 s TWT). There are several strong amplitude reflectors of varied morphology throughout unit 2A, except for the irregular parts (Fig. 4, CDPs 19,609–20,209 at 4.2–5.0 s TWT). Compared to unit 2A, unit 2B shares many characteristics, but may be distinguished by its more pronounced mounded morphology (Fig. 4, CDPs ~19,609 in unit 2B) with locally lower frequency and higher amplitude seismic reflectors. An incision cuts through T2 down to the top of unit 2A (Fig. 4, CDPs 16209–18209 at 3.1–3.8 s TWT), and is distinguished by its much higher amplitude boundary which cuts the pre-T2 reflectors. A set of channel-like incisions are of great prominence (Fig. 4, CDPs 18709–20709 at 4.1 s TWT), and overlies a sedimentary package with more or less chaotic, mostly weak amplitude and poor continuity

reflectors (Fig. 4, CDPs 19409–20769 at 4.2 s TWT).

Seismic unit 3A lies between unconformities T1 and T2. In the northwest, the sub-parallel reflectors are similar to those in the lower units but are truncated by T1, underlying chaotic and discontinuous reflectors (Fig. 4, CDPs 14209–15209 in unit 3A). The infilling reflectors show much higher amplitudes, with a quite good continuity in each period. Close to the MFZ, the unit is characterized by successive parallel reflectors with generally high but locally variable amplitudes, onlapping landward onto unconformity T2 that drops about 1.0 s TWT within 18 km in this area (Fig. 4, CDPs 18609–2100 at 3.2–4.3 s TWT). At the top of the unit, reflectors are truncated by the channel-like incision of unconformity T1. Deposits of unit 3A show a highly variable thickness ranging from 0 to 0.8 s TWT.

The youngest unit 4A, in contrast to other units, is dominated by the relatively low amplitudes within the entire sequence, in some parts being almost transparent. Continuous reflectors with low frequency onlap onto unconformity T1 at the base of the unit and are truncated at the sea floor. Overall reflection configuration is aggradational (Fig. 4, CDPs 14209–17009 at ~3.2 s TWT). In some place at the seaward end of the profile, the acoustic facies are defined by several channel-like incisions filled with relatively young sediments with sub-parallel reflectors that onlap onto the flanks of the incisions (Fig. 4, CDPs 17409–18809 at ~3.2 s TWT). Sub-parallel continuous reflectors become patchy and hummocky towards the southeast (Fig. 4, CDPs 18809–20809 at ~3.6 s TWT). The erosive terrace-like seafloor morphology is generally smooth but locally presents incision features.

4.1.2. Mozambique Fracture Zone

Crossing through N-S trending Mozambique Fracture Zone (Fig. 1b), the seismic profile shows a distinct difference in sediment thickness between the CT and the MB (Fig. 5), which obscured the horizon picking. Within the MFZ, the basement is faulted and thus discontinuous and irregular (Fig. 5, CDPs 20809–21809 at 5.0 s TWT). The total sedimentary thickness is less than 1.0 s TWT (Fig. 5, CDPs 20809–21709 at 4.2–4.5 s TWT) and can be divided into two units. Seismic unit A is constructed of a set of parallel-subparallel reflectors with moderate-weak amplitude and generally good continuity. Lying above the basement, part of this unit appears to have been uplifted (Fig. 5, CDP 20809 at 4.6–4.8 s TWT) thus the whole sequence exhibits S-shaped deformation characteristics (Fig. 5, CDPs 20809–21409 at 4.4–4.9 s TWT). In the seismic unit B, its lower part consists of more or less well-layered reflectors, with moderate-weak frequency and a thickness less than 0.3 s TWT, while in the overlying upper part, the majority of the reflectors

Table 2
Stratigraphic discontinuities and depositional units defined by Du Toit and Leith (1974), Dingle et al. (1978), Martin et al. (1982), Martin et al. (1982), Fischer et al. (1982) and Fischer et al. (2016); Fischer and Uenzelmann-Neben (2018) and its correlation with the proposed stratigraphic scheme and ages in the southern Mozambique continental margin. “H” represents the hiatus without a given name.

This study	Du Toit and Leith, 1974	Dingle et al. (1978)	Martin et al. (1982)	Preu et al. (2011)	Fischer et al. (2016); Fischer and Uenzelmann-Neben (2018)	Age constrain
Major seismic units and depositional units	Major hiatus	Units and discontinuities Unit3	Major discontinuities L	Major discontinuities L	Units and hiatus S2b	Middle Miocene-Quaternary
Seismic unit 4		Angus	Jimmy H ₀ Angus	Jimmy Angus		
T1	H ₁				H ₃	Early/middle Oligocene-early Miocene
Seismic unit 3						
T2	H ₂		C/T Boundary			Paleocene-Eocene End of Cretaceous
Seismic unit 2		Unit2			S2a H ₄	Late Late Cretaceous Middle Late Cretaceous Cenomanian-Turonian Early Cretaceous
T3		McDuff Unit1	McDuff	McDuff	S1	
Seismic unit 1	1B 1A					
Basement						Pre-Cretaceous

are chaotic with low continuity, or nearly reflection free (Fig. 5, CDPs 20809-21609 at 4.1–4.4 s TWT), overall showing a block-like feature. At the surface, the present-day seafloor is locally mounded-wavy, with varied amplitude reflection patterns.

4.1.3. Mozambique Basin

Two regional unconformities named as t1 and t2 within the MB are both based on clear seismic facies changes described below. Onlapping reflection of overlying strata is widespread at both t1 (e.g., Fig. 6, CDP 24473 at 6.0–6.2 s TWT; CDPs 26273-27473; 31673-32273 at 6.0–6.4 s TWT) and t2 (e.g., Fig. 6, CDPs 28973-29873 at 6.5–6.9 s TWT), except for areas with chaotic reflectors (e.g., Fig. 6, CDPs 26573-27473 at 6.5 s TWT).

Seismic unit 1b is characterized by discontinuous and sub-parallel reflectors of weak amplitudes, showing locally layered or chaotic patterns (Table 2). Its basal boundary tg was faulted near a basement high (Fig. 6, CDPs 30,473–32,273 at 6.2–7.1 s TWT), which appears to have confined distribution of sediments in this area. The depocenter was located in the depression generated by the topographic disparity, just NW of the basement high, the depositional thickness thins with onlapping reflectors (Fig. 6, CDP 29873 at 7.1 s TWT).

Seismic unit 2b can be distinguished by distinct differences in seismic reflection characteristics. Close to the MFZ, sedimentary packages are of chaotic, highly disrupted and almost transparent reflection pattern (Fig. 6, CDPs ~29230 in unit 2b), extending over 40 km with an average thickness of 0.3 s TWT. These deposits laterally merge into very well-stratified reflectors (Fig. 6, CDPs 29973~ at 6.5–7.0 s TWT). A sedimentary sequence characterized by a set of sub-parallel reflectors with variable amplitudes and moderate continuity fills the depression (Fig. 6, CDPs 28973-31073 at 6.5–7.0 s TWT). An undulating pattern of reflectors can be observed above the basement high (Fig. 6, CDPs 31073-32573 at 6.4 s TWT).

Seismic unit 3b has mostly sub-parallel layers with slightly stronger amplitude and moderate-highly continuous reflectors compared to the lower units. Its basal boundary t1 behaves as a well-marked regional unconformity with local wavy morphology (Fig. 6, CDPs 30773-32573 at 6.0 s TWT), marking a change in sedimentation style. Wedge-shaped features with internal downlapping reflectors are observed (Fig. 6, CDPs ~23,273 at ~5.9 s TWT). Seaward, there are a series of sub-parallel reflectors showing onlap or truncation reflection pattern in different periods (Fig. 6, CDPs 29873-32573 at ~6.5 s TWT).

4.2. Age model

Based on several studies introduced above, a general seismic stratigraphy for the study area has been developed. A summary and comparison of stratigraphic frameworks and their horizon nomenclature are given in Table 2. Major seismic horizons and the seismic units defined in the continental margin area of this study were correlated, utilizing their seismic facies, with the results of these former studies to establish a stratigraphy in our study area. Following this stratigraphy, T3 marks the boundary from Lower Cretaceous to Upper Cretaceous, T2 is assigned to the end of Cretaceous, T1 developed in the early-middle Oligocene to the middle Miocene. Being consistent with the interpretation of the origin of the boundary Tg as the onset of continental rifting, we propose that the basement was formed before the Lower Cretaceous.

For the stratigraphy within the MB, we mainly use the DSDP 248 well data analysis results as a reference for comparison (Table 3). In this way, underneath tg the basement was formed at around the end of the Cretaceous, t2 represents the early-middle Paleocene unconformity and t1 marks the hiatus from late Eocene to early-middle Miocene.

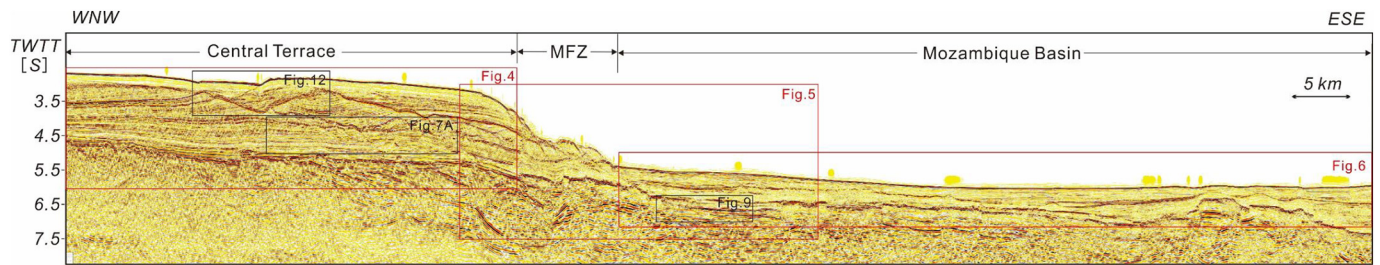


Fig. 3. Uninterpreted whole seismic profile from the NW to SE. The Central Terrace part, Mozambique Fracture Zone and the Mozambique Basin part are presented by two black solid lines. See location in Fig. 1b.

5. Morphosedimentary features and sedimentological interpretation

5.1. Gravitational features

Both the CT and the MB host numerous gravitational features including gravity-driven post-depositional deformation, such as slides, slumps and slope creep, and those related to active down-slope sedimentary processes, such as mass-transport deposits and turbidites.

a) Slide/slump

In Seismic unit 2A, a rotational landslide complex is cut obliquely by the seismic profile. A series of three rotated blocks 0.3 s thick are bounded by listric faults that sole out on a basal glide plane overlying undeformed strata. Downslope, the slide complex passes into stratified sediment with low undulations (Fig. 7B). It is not clear whether this is a compression zone downslope from the slide, or whether the seismic line

is oblique to the slide direction and the faulted zone with fluid chimneys represents the lateral edge of the slide. The total amount of movement on the identified slide blocks is small: they have essentially rotated in place and are thus similar to rotational slides reported by He et al. (2014) and Sun et al. (2017a). The slide feature is not a sediment wave assemblage in which the troughs mimic faults (Lee et al., 2002). The putative waves are irregular in their architecture, with very different climb angles for successive putative troughs. Upslope, no sediment waves are visible, only a small headscarp ~0.05 s high.

Sliding and erosion also took place at the present sea-floor adjacent to the fault zone at the eastern margin of CT. Sliding started from the steepest position on the escarpment and then deposited on a relatively broad and gentle platform, with the total flow distance up to 700 m (Fig. 8b). There were multiple periods in this gravity driven slope failure process, as the headwall scars formed in different stages with step-forming detached sediment masses (Fig. 8b).

b) Creep

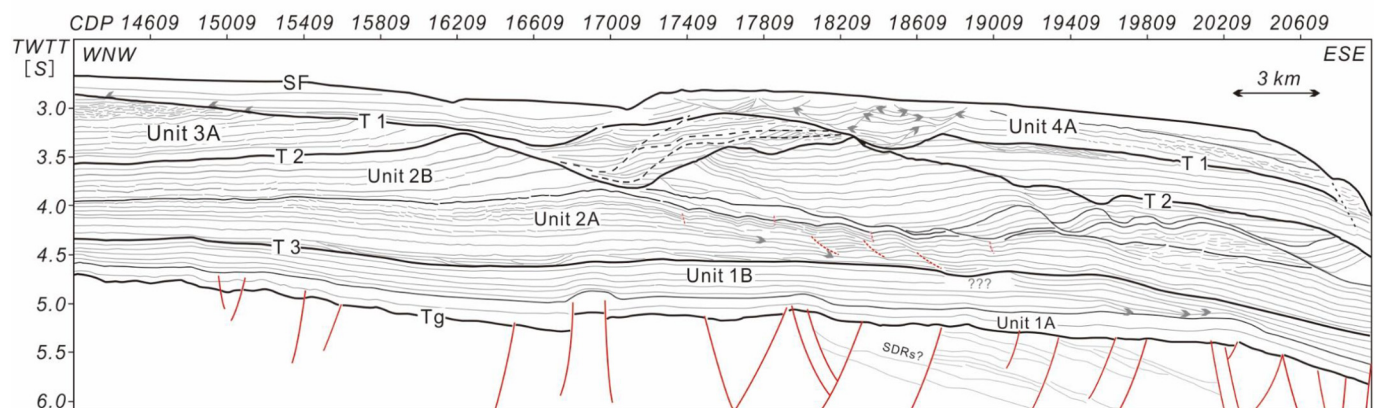
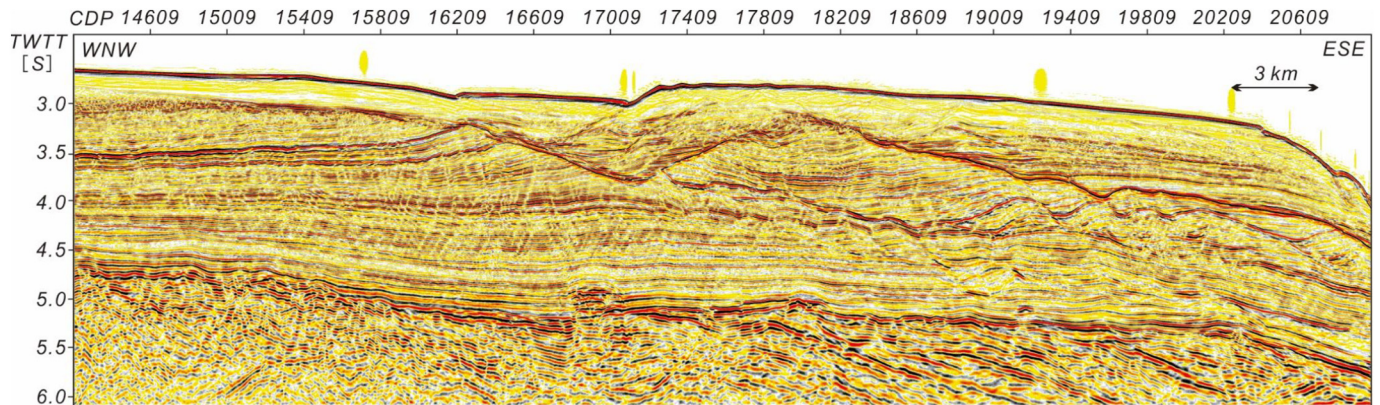


Fig. 4. Seismic profile within the CT part showing major morphosedimentary features, stratigraphic units and discontinuities with assignments for the Early Cretaceous - Late Cretaceous boundary (T3); end of the Cretaceous (T2) and early-middle Oligocene (T1). See location in Fig. 3.

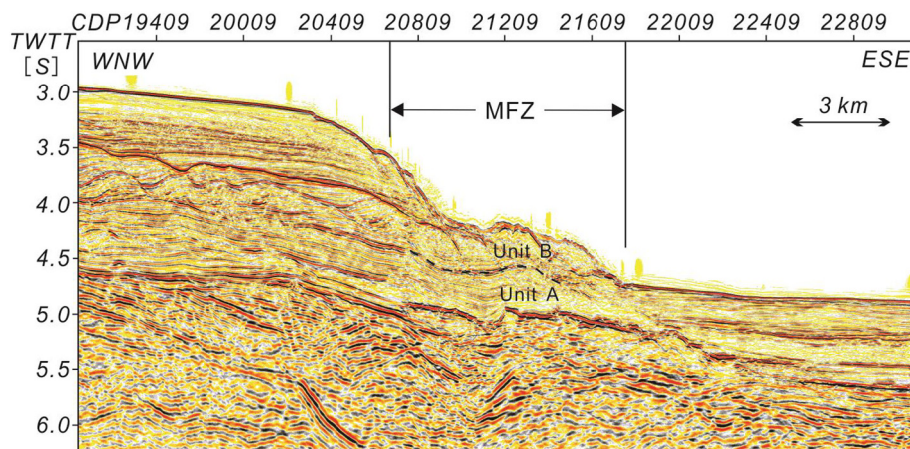


Fig. 5. Seismic profile crossing the MFZ show that an escarpment occurs on the flank of CT. Different sequences and sedimentary thickness on its two sides are presented. See location in Fig. 3.

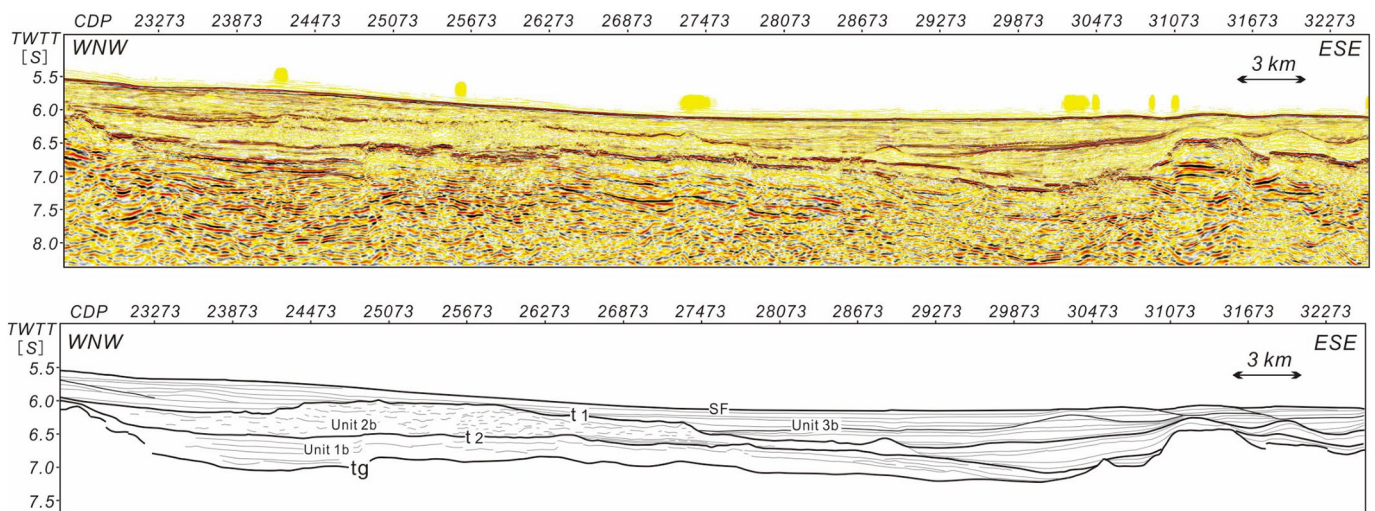


Fig. 6. Seismic profile within the MB part showing the major morphosedimentary features. Stratigraphic units and discontinuities are shown, with assignments for the early-middle Paleocene (t2) and late Eocene to early-middle Miocene (t1). See location in Fig. 3.

In Seismic unit 2A, upslope from the landslide, a wavy feature above an irregular possible decollement surface is interpreted as creep (Fig. 7A). The wavelength of the undulations is 1–2 km and they consist of parallel seismic reflectors with moderate frequency and fairly strong amplitudes. The creep packet is composed of a number of elongated undulations which contain crests defined as ridges and depressions defined as troughs. The troughs themselves are symmetrical, although their upslope flanks are slightly steeper than their downslope flanks due to the tilting of the slope. The crest alignments are erect and the upslope and downslope flanks have almost the same sediment thickness of 0.1 s TWT, with no upslope migration displayed. This group of wavy sediments is most likely caused by slow gravity-driven slope creep, based on three pieces of evidence: (1) they appear to have an underlying

irregular decollement surface; (2) the ridge and trough on the lower slope are of equal size and equally symmetrical compared to those on the upper slope, so there is no increasing downslope size or asymmetry, which is one of the typical features of sediment waves produced by turbidity currents (e.g., Lee and Chough, 2001; Symons et al., 2016); and (3) small faults are associated within some troughs, whereas current-formed sediment waves are more or less continuous without faulting (Wynn and Stow, 2002; Lee et al., 2002).

c) Mass transport deposits

Stacked sediment bodies manifested as chaotic to transparent internal reflection pattern are observed between the locally irregular

Table 3

Stratigraphic discontinuities and depositional units in the Mozambique Basin based on the correlation to the nearby DSDP sites 248 (Schlich, 1974).

This study	DSDP 248	Age constrain
Major seismic units and discontinuities	Major lithologic units and hiatuses	
Seismic unit 3b	Unit I	Middle Miocene-Quaternary
t1		Late Eocene to early-middle Miocene
Seismic unit 2b	Unit II	Eocene
t2		Early-middle Eocene?
Seismic unit 1b	Unit III	Possible Paleocene/early Eocene
Basement	Unit IV	Pre-end of the Cretaceous

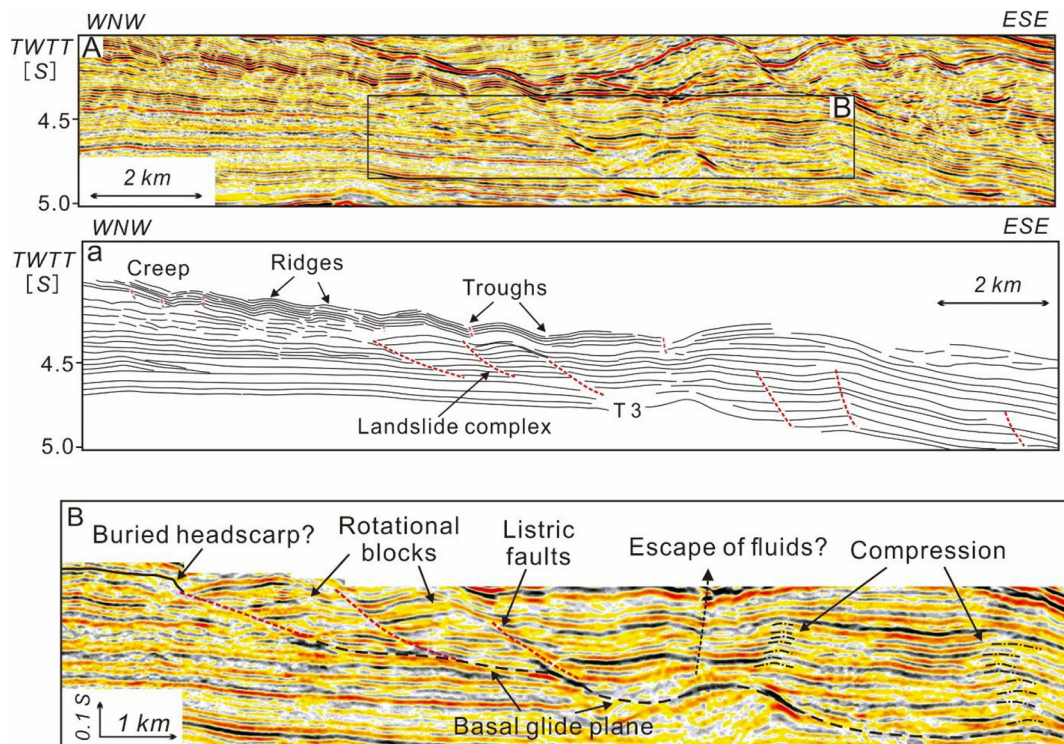


Fig. 7. (A)-(a) Seismic profile showing the boundary of T3 (Early Cretaceous - Late Cretaceous boundary) and two groups of wave-like sediments that interpreted as creep and landslide complex. See location in Fig. 3. (B) Seismic features with the interpretations. The buried headscarp (black solid line), possible basal glide plane (black dotted line), listric faults (red dotted line) and the rotational blocks in-between suggesting the nature of retrogressive failure of the landslide. See location in panel A. (For interpretation of the references to colour in this figure legend, the reader is referred to the web version of this article.)

boundaries of t1 and t2 in the MB (Fig. 8c), and they are bounded above, below and laterally by continuous and weakly deformed strata (Fig. 8c, d). Through comparing these seismic reflection characters to the those from other studies (e.g., Moscardelli et al., 2006; Bull et al., 2009; Alves, 2015; Sun et al., 2017a, 2017b) interpreted as mass-transport deposits (MTDs), the results show very close similarity, such

that the sediment bodies in this study are interpreted as MTDs. The three stages of MTDs observed have a total length up to 40 km and varied thickness from 0.1 to 0.6 s TWT (Fig. 8a). Seaward, the MTDs pinch out and merge into stratified reflector packages, interpreted as turbidite and hemipelagite sequences. Related elements including basal shear surface and concave up glide plane are identified, marking the

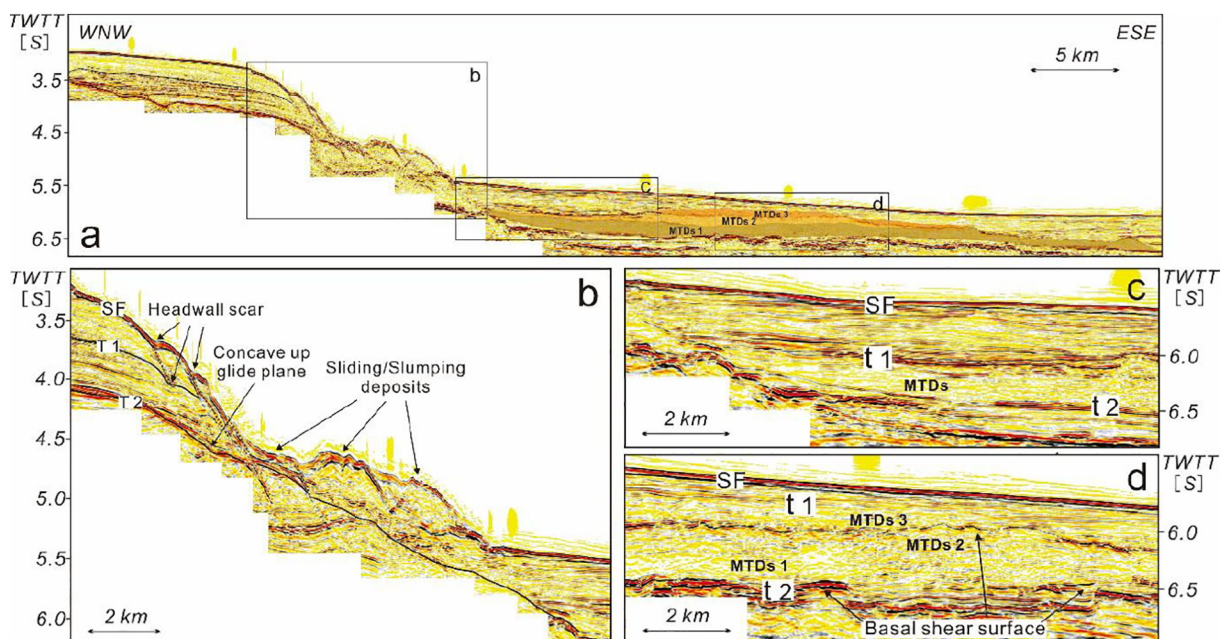


Fig. 8. (a) Seismic profile showing the dimension of multi-stage MTDs (colored block mass) in the MB. (b) Typical seismic features of the elements interpreted as slides/slump deposits. (c) Seismic profile showing the location of MTDs in unit 2b (between t1 and t2). (d) Seismic profile showing the basal shear surface and different stages of the MTDs.

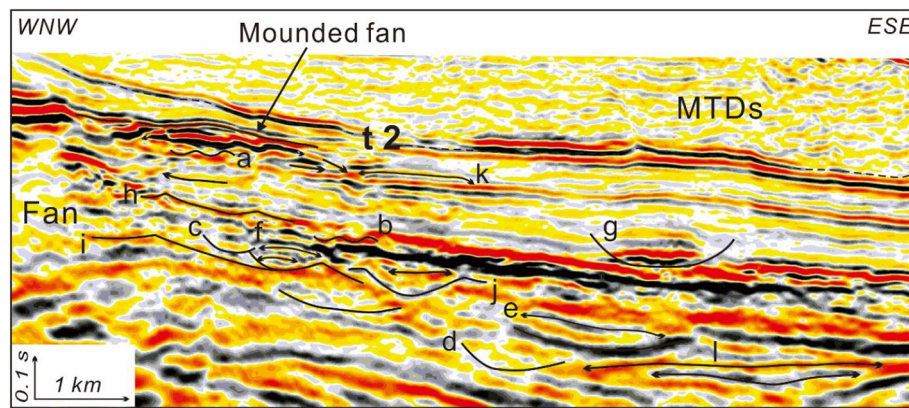


Fig. 9. Typical seismic expressions showing architectural elements building up a submarine fan system in the MB, which include a and b: small scale channel; c, d, e: channel in-filling deposition; h, i, j: channel-levee complex; k and l: proximal lobe. See location in Fig. 3.

local boundaries t2 and T2, respectively (Fig. 8b, d).

d) Submarine fan systems

Below t2, discontinuous reflector packages occupy parts of the unit 1b near the MFZ in the MB. Intervals of irregular reflections of both moderate amplitude reflection patterns are interpreted as small scale channels (e.g., a and b in Fig. 9). Isolated or stacked U/V shaped incisions cutting into underlying reflectors with width at around 1 km are typical channel-form incisions, within which is channel in-filling deposition, characterized by short parallel reflectors with varied amplitudes (e.g., c, d, e in Fig. 9). Some of these in-filling reflectors show upward convex geometry (e.g., f in Fig. 9), which may be the result of differential compaction between mud and sand (e.g., Revil et al., 2002). Compared to much of the channel infill characterized by reflectors with moderate and homogeneous amplitude and interpreted as more mud-rich (e.g., c and d in Fig. 9; Mayall et al., 2006), packages of discontinuous high amplitude reflectors occurring at the channel bases (e.g., g in Fig. 9) may correspond to coarser components carried in the lower parts of turbidity currents (Kneller and Buckee, 2000). The combination of channel forms and channel in-fillings forming the channel belt complexes, and some with distinctive external levees that are characterized by moderate-low amplitude reflection patterns in wedge-shaped depositional geometries, is thus interpreted as channel-levee complexes (e.g., h, i, j in Fig. 9) in a base of slope fan. Relatively long high-moderate amplitude reflection patterns are interpreted as proximal lobes (e.g., k and l in Fig. 9), which could be thick beds of fine/medium grained sands (Flood and Piper, 1997). All these facies are architectural elements building up a submarine fan system in the study area, which share many characteristics with the architectural facies in the upper-middle part of fans from many other studies (e.g., Deptuck et al., 2003; Schwenk et al., 2005).

The horizon t1 that marks the early-middle Miocene hiatus is fairly continuous with strong amplitude, covering a large area of the MB. Above T1, seismic reflectors are relatively continuous and of moderate amplitude, so that reflector stratification is clearly visible (Fig. 10b, c, d). Below T1, chaotic reflection packages (MTDs) occupy part of Unit 3b (Fig. 10a), the rest of which is mainly composed of irregular weak amplitude reflectors (Fig. 10b, c, d), while more or less continuity could be observed in some regions (Fig. 10e, d). All of these phenomena clearly indicate a marked sedimentary facies change at around the middle Miocene. Widely identified onlapping reflection patterns with relatively high amplitudes (Fig. 10a, d) and U-shaped channel-form incisions (Fig. 10b, d) are typical seismic features of turbidite systems. This would correspond with an increased terrigenous influence, including clays, silts and coarse sands, of Miocene to Pleistocene age encountered by DSDP 248 (Schlich, 1974). Particularly, there are

turbidites trapped in the troughs of wavy reflectors, distinguished by their higher amplitude with onlapping reflection pattern (Fig. 10e), which probably are coarser-grained material carried in the lower parts of turbidity currents. Similar facies are reported off the southern margin of the Orinoco Valley (Ercilla et al., 2002).

5.2. Contourite features

Evidence of along-slope sedimentary processes is quite common, based on the identification of multiple contourite features, which include depositional (drifts and sediment waves), erosional (erosive surface, moat, valleys), widespread hiatuses, and mixed (contourite terrace) features. Contourite drifts, as the main result of sediment accumulation controlled by bottom current activity, are well-recognized through their external geometry and internal reflector character. Erosional features typically occur associated with truncated reflectors and, in particular, large-scale erosive surfaces can be related to the regional unconformities, which have been identified, dated and used to establish the age model. The mixed features refer to contourite terraces, which display as a more or less flat surface tilted basinwards and partly covered with both depositional and erosional features.

5.2.1. Depositional contourite features

Six drifts (drifts 1, 2, 3, 4, 5 and 6) with different dimensions occur on the continental margin (Fig. 11a). Vertically stacked mounded-elongated drift 1 and 2 occupy positions within seismic units 2A and 2B, respectively. Drift 1 is at least 40 km long and up to 0.7 s TWT thick. As a whole it was built on a relatively flat base and shows a sediment accumulation regime change with a clear sedimentation rate peak at the crest, which indicates bottom current control, leading to the interpretation of drifts. Drift 2 has a similar maximum thickness but may have lost accumulated sediments, due to the truncation on its SE side. Both drifts show progradational and aggradational internal reflection configurations and are characterized by more or less well-layered reflectors, but are commonly disrupted by fluid-escape features, which are evident as vertical stripes of transparent material.

Drift 2 differs from drift 1 with a higher inclination of reflectors. Seaward, the reflectors have apparently concave upward tendency, based on which we suggest potentially another smooth mounded drift 3 that is hosted on the SE side in seismic unit 2B, close to the MFZ, before it was eroded (Fig. 11a). Sheeted drifts 4 and 5 span 15 km in length and together make up unit 3A. Drift 4 reaches sedimentary thicknesses of up to 0.5 s TWT, its internal reflectors are similar to those of drift 2 but more irregular. In general, drift 5 has a stronger amplitude reflector pattern with a relatively uniform thickness of 0.4 s TWT. Between drift 4 and 5, a local mounded configuration is also developed inside of the V-shaped incision (Fig. 12). Located at the edge of the present-day sea

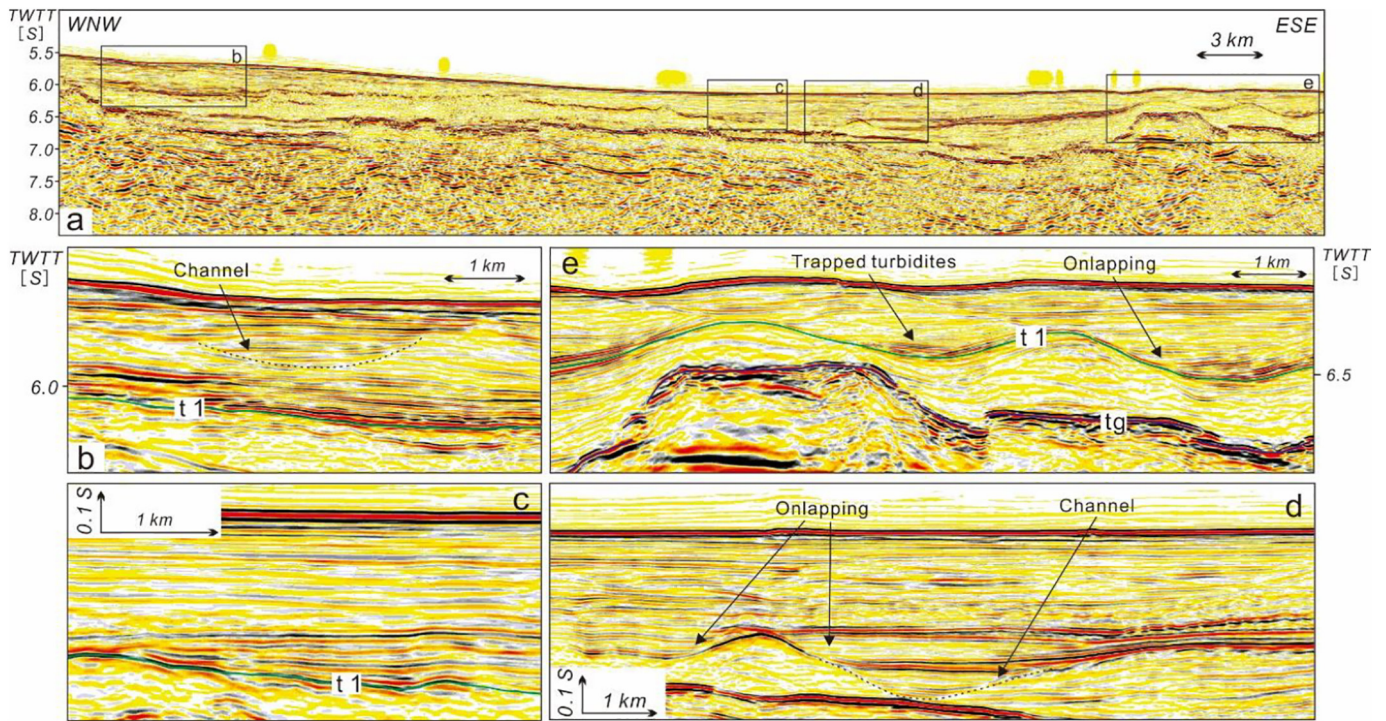


Fig. 10. (a) Seismic profile showing typical seismic features of turbidites (See location in Fig. 3), with (b) Channel incision cutting into underlying reflectors; (c) Seismic reflection pattern of onlapping contacts against the underlying reflectors; (d) Channel incision and infill with onlapping seismic reflection pattern; (e) High amplitude reflectors trapped in the troughs of wavy reflectors.

floor, elongated plastered drift 6 extends in a downslope direction at ~2250–2600 m water depth. The sedimentary crest of the drift runs parallel to the lower slope and reaches a height of 0.2 s TWT.

Sediment waves appear most commonly within drifts 5 and 6, as fields close to the edge of escarpment, at ~2250–2900 m water depth

(① and ② in Fig. 11a). These wavy bedforms are relatively small-scale; each wavelength is about 200 m and the observed maximum wave height is less than 10 ms TWT (Fig. 11b, c). Most waves within drift 5 are scattered in the middle of layered strata, show asymmetric and irregular characteristics, but undulations are low (Fig. 11b). Undulations

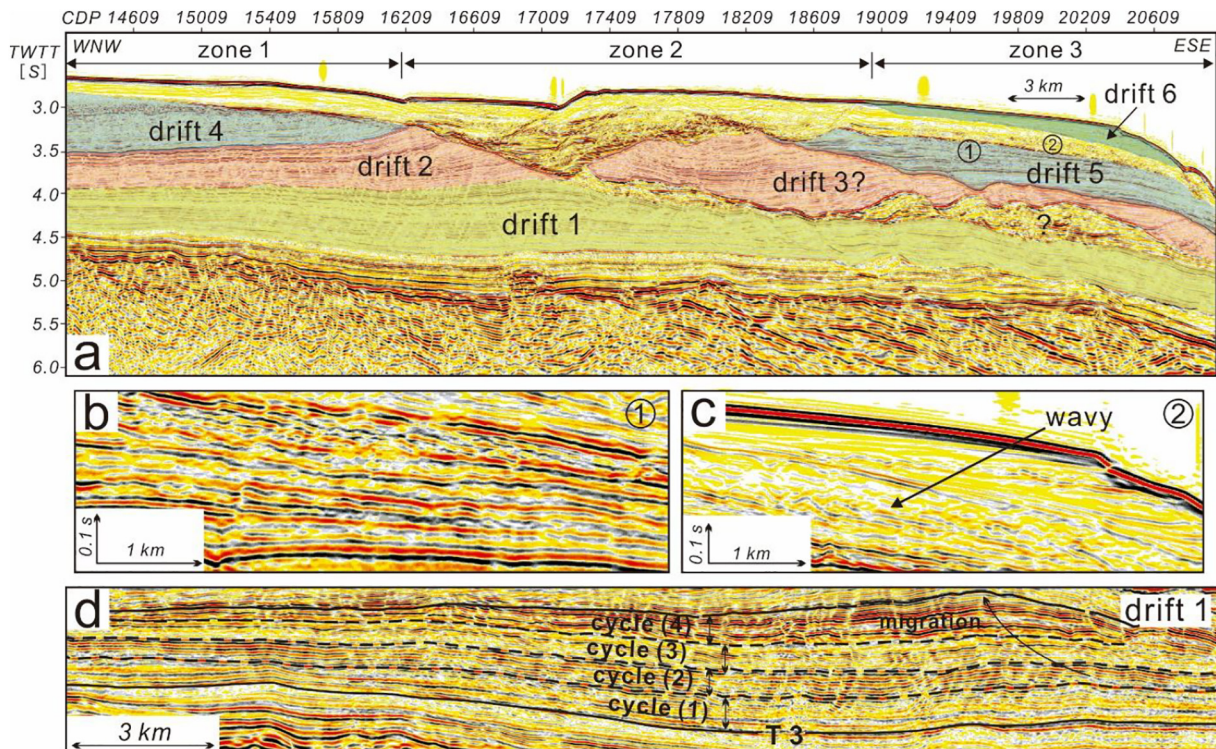


Fig. 11. (a) Seismic profile within CT part showing different zones of terrace and locations of drifts (colored blocks). (b)-(c) Wavy seismic features of sediment waves. (d) Seismic profile of drift 1 showing cycles and migration features.

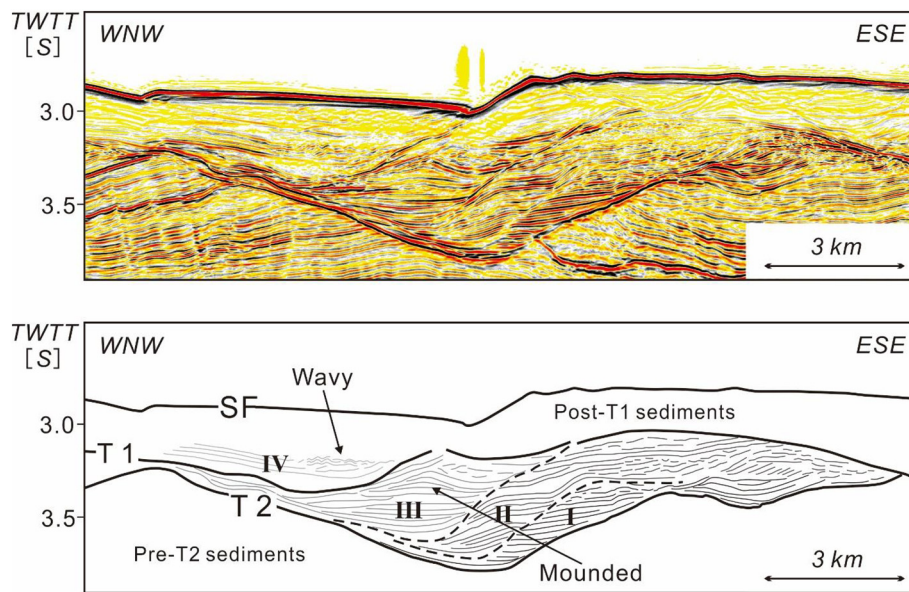


Fig. 12. Morphosedimentary features of canyon showing mixed erosive and depositional processes. Four stages of canyon fill are presented with solid line in black from deep to shallow, which corresponding to each stage. See location in Fig. 3.

within and underlying drift 6 are of weaker amplitude, and they appear to migrate upslope or downslope (Fig. 11c).

5.2.2. Erosional contourite features

A large-scale erosional surface dominated by well-defined truncation reflections is identified within part of T1 boundary, extending over 15 km and clearly marks the variation of seismic reflection characteristics from generally moderate-strong to weak amplitude reflectors and to transparent seismic packages in parts. More obvious truncation occurs with a U-shaped contourite moat 3 km wide and 0.2 s TWT in depth, associated with local mounded elongated drift above the sheeted drift 5 (Fig. 4, CDPs 18,209–19,009 at 3.1–3.3 s TWT). Moat infill appears as layered reflectors with variable amplitude, among which are mixed reflectors with a clinoform-like progradational pattern. Above this moat, there is a group of V-shaped valleys vertically and horizontally truncating the underlying and lateral strata in seismic unit 4A (Fig. 4).

5.2.3. Mixed contourite features

Located on the lower slope in ~2000 m water depth, the CT is characterized by a gentle gradient and smooth topography. Its general morphology and setting indicate it is a contourite terrace (e.g., Hernández-Molina et al., 2010, 2016; Preu et al., 2012, 2013; Thiéblemont et al., 2019; Yin et al., 2019). The terrace shows a clear high amplitude reflection pattern, and terminates to the southeast in an escarpment. The CT can be subdivided into three zones (Fig. 11a): zone 1 of the terrace is characterized by mostly horizontal layered reflectors with uniform thickness; zone 2 is in the middle part where truncated reflectors indicate erosive processes; and zone 3 located in the distal domain encompasses a major plastered drift.

6. Discussion

6.1. Evolution of the Mozambique margin

6.1.1. Restricted marine sedimentation during the Early Cretaceous

The aggradational stacking pattern of seismic unit 1A showing successive deposition, suggests at this period the MB was subjected to ongoing subsidence after the initial break-up. Accompanied by the regional transgression (Flores, 1973; Girdley, 1974), a deep-water setting developed no later than the late Early Cretaceous in the study area,

based on the foraminifera genera *Citharina*, *Lingulina* and *Marginulina* at DSDP Site 249 that are all the markers of a deep-water sedimentary environment (Quilty, 2011; Youssef and El-Sorogy, 2015; Ustinova and Tesakova, 2017).

The lack of current indications suggests relatively restricted conditions, in agreement with the occurrence of widespread black shales (Lower Domo Shales Formation in the Lower Cretaceous) in the central-southern parts of the MB (Nairn et al., 1991; Salman and Abdula, 1995). Such black shales are also present in the Falkland/Malvinas Basin (Baby et al., 2018) and along the conjugate margin in the Weddell Sea (see Africa-Antarctica Corridor tectonic setting map shown by Mueller and Jokat, 2019), where they have been attributed to deposition in an anoxic environment (e.g., Meyers, 2006; Izumi et al., 2012). At DSDP Site 249, organic carbon rich layers of Early Cretaceous age (Simpson et al., 1974) were also deposited in an oxygen-depleted environment (Girdley, 1974; Vallier and Kidd, 1977). Such conditions exist in areas with at least partially restricted oceanic circulation, that are isolated from the open sea (Jones, 1982; Wignall and Bond, 2008). Overall, it can be inferred that the similar restricted and potentially-euxinic conditions prevailed not only in the southern MB, but also most of the evolving Indian Ocean during the Early Cretaceous.

The stratigraphic pattern of the slope system is characterized by slope clinoforms in unit 1B (Fig. 4), as sediment input from rivers bypassed the topsets and reached the flat bottomsets, prograding with a very low-angle trajectory (Steel et al., 2002). In this way, we propose in the Early Cretaceous the southern MB was more or less an isolated basin with slope clinoforms developed.

6.1.2. Open marine sedimentation during the Late Cretaceous

Above T3, seismic unit 2A was deposited with depocenters in the middle part of the CT (Fig. 4, CDP 17009 at 3.8–4.5 s TWT), forming symmetrically mounded geometry. This kind of sediment mound in a deep-sea slope setting is generally distinguished as either an unchanneled lower fan (Normark, 1970; Mutti, 1977) or as contourite drifts (Stow and Mayall, 2000; Stow et al., 2008; Faugères and Stow, 2008). Both slope lower fan and mounded drift can reach tens of kilometers (length/width scale), with internal reflection character of downlap terminations. Nevertheless, there are still some established criteria can be followed to distinguish down-slope and along-slope depositional process.

Firstly, a distal fan is an area of turbidity current deposition free of

channel features (Normark, 1978). Typically, it is characterized by a lobe complex of superimposed multi-staged sedimentary lobes and displays more than one stacking pattern (progradational, aggradational or retro-gradational stacking of lobes) (e.g., Hodgson et al., 2006, 2016; Mulder and Etienne, 2010; Marchès et al., 2010). Due to the specific property of gradually weakening energy in turbidity flow (Normark et al., 1980; Lee et al., 2002), in most cases, seismic facies in terminal lobes show varied features within stratified sediments (e.g., Zhou et al., 2015; Zhang et al., 2016; Huang et al., 2019).

However, these diagnostic criteria do not appear within unit 2A. Rather, three seismic traits observed are more compatible with a contourite drift interpretation: firstly, the seismic features are quite uniform, and generally sediments accumulated in a layered aggradational stacking pattern (Fig. 11d); secondly, the presence of slateral migrating crests indicate an elongation direction, as is universal within contourite mounded-elongated drifts (e.g., Bianchi and McCave, 2000; Wildeboer Schut et al., 2002; Van Rooij et al., 2007) due to the Coriolis effect, current intensity change and the interaction with the morphology (Faugères et al., 1999; Faugères and Stow, 2008); and thirdly, detailed observation shows a cyclicity in seismic facies is present (Fig. 11d), notably: (1) smooth, parallel reflectors of relatively weak amplitude or even transparent at the base; (2) moderate-to-high amplitude reflections in the upper part; (3) an amplitude weakened zone similar to the base and (4) a high-amplitude continuous surface at the top. This seismic cyclicity resembles that of the drifts developed in the Gulf of Cadiz, where periodical changes in seismic facies are most likely synchronous with lithologic change related to bottom-current variability (Llave et al., 2001, 2006). As such, we suggest that seismic unit 2A represents contourite drift deposition. Based on the classification of Faugères and Stow et al. (2008), we further identify it as a plastered drift with a giant mounded elongated shape (drift 1) that is typically developed on a gentle slope (Faugères and Stow, 2008). Observations from Iceland Basin of Gardar Drift (Bianchi and McCave, 2000; Elliott and Parson, 2008) with a similar shape support this interpretation.

The existence of drift 1 as a long-term depositional product indicates a relatively stable bottom current flow, which is consistent with the appearance of the regionally developed mid-Cretaceous horizon McDuff (T3) that is considered to represent the beginning of an open marine sedimentation regime (Dingle et al., 1978; Martin et al., 1982). The current flow may have resulted from the opening of one or more oceanic gateways due to tectonic movements, such as southward drifting of the Astrid Ridge no later than 100 Ma and the deepening of the passage south of the Agulhas Plateau since ~90 Ma (Castelino et al., 2016). A similar setting associated with bottom current activity has been reported in the nearby area of MozR, where the beginning of intense circulation is interpreted to account for the ~25 Ma ridge-wide hiatus documented in the sedimentary record from ~100–75 Ma (Fischer and Uenzelmann-Neben, 2018). To the north, Castelino et al. (2015) described the observed sediment wedges and the sediment waves with wide regional distribution of over 70 km to the Late Cretaceous onset of north-south bottom current activity in the northern MB. Also, the Somali Basin is suggested to have been a current-swept basin in Late Cretaceous times (Coffin et al., 1986). It can be inferred that water mass circulation along the Mozambique margin in the Indian Ocean was already established in the Late Cretaceous, although it is not clear whether it is similar to the present-day oceanographic setting (Stage A in Fig. 13).

Offshore from the northern and southern Mozambique margins, sediment accumulation characteristics reveal that the surface circulations (MC) began in the Early Miocene (Walford et al., 2005; Preu et al., 2011), and deep circulation (NADW and AABW) did not commence before late Eocene times in nearby Transkei Basin and Natal Valley (Fig. 1a; Ben-Avraham et al., 1994; Niemi et al., 2000; Schlüter and Uenzelmann-Neben, 2008). Therefore, we tentatively assume that an intermediate-depth circulation was responsible for current activity in the study area, which is in accordance with the palaeodepth of

1600–1800 m suggested by Castelino et al. (2016) for the CT.

6.1.3. Down-slope processes dominated sedimentation during the Paleocene-Eocene

We interpret a change and probable reduction in bottom-current activity during the Paleocene-Eocene. That some weak current activity persisted is indicated by the appearance of sheeted drifts 4 and 5 (Fig. 11), which are typically deposited by broad non-focused and relatively low-velocity currents from 3 to 10 cm/s (Stow et al., 2008; Faugères and Stow, 2008). Contourites with higher amplitude reflections (Fig. 4, CDPs 18,809–20,609 at 3.3–3.6 s TWT) suggest a sand-rich deposit in a depositional/erosional body linked with a zone of higher energy flow (Faugères and Stow, 2008; Stow et al., 2009, 2013), such as that located on the edge of the margin. Furthermore, the underlying T2 boundary may have acted as a rough surface contributing to turbulence of the flow (e.g., Hernández-Molina et al., 2006; Wang et al., 2018).

However, the identified MTDs on the MB (Unit 2b in Fig. 6) are clear evidence that down-slope processes were active at this time and probably dominated deep-water sedimentation. Other evidence for down-slope processes is listed below.

a) Contourite-related submarine glide plane

Close to the MFZ, part of the T2 horizon is characterized by a 20 km long erosional surface (Fig. 4, CDPs 18409–20609 at 3.1–4.4 s TWT) with strong amplitude and dipping seaward. This local erosional surface is interpreted as a consequence of both mass transport processes and bottom current scour, based on the following evidence: (1) the adjacent steep escarpment that is prone to slope failure; (2) MTDs that thin towards the southeast in the MB, which indicates the onset of this mass wasting processes originated from the Mozambique continental slope; and (3) a 2 km wide V-shaped incision at the base of steepest part (Fig. 4, CDPs 19409–19609 at 3.8 s TWT), which is quite abnormal even in the concave up glide plane and appears more like a contourite channel. The relative importance of mass transport processes and bottom current scour is uncertain. On the one hand, bottom currents can favor the sediment supply to build up a relatively steep flank, then potentially triggering the down-slope processes (e.g., Habgood et al., 2003; Hanquiez et al., 2010). On the other hand, slides or slumps with various triggers (Locat and Lee, 2002; Sultan et al., 2004) on the steep slope could directly affect the bottom current flow velocity and lead to local erosion/non-deposition (Stow et al., 2008; Hernández-Molina et al., 2008).

b) Canyon system associated with bottom current effect

The V-shape incision, characterized by a continuous and strong amplitude reflector, cuts the adjacent strata, and marks deep erosion up to 0.63 s TWT depth with a maximum width about 10 km on this seismic profile (Fig. 12), although the channel may have been traversed obliquely in the survey. These features in deep sea settings are commonly distinguished as channels eroded by gravity flows (e.g., He et al., 2013; Gong et al., 2013; Wang et al., 2018) or bottom currents (e.g., Faugères et al., 1999; Faugères et al., 2002; Vandorpe et al., 2016). In most cases, marked erosive features from bottom currents corresponding to higher energy occur where bottom currents impinge onto topographic obstacles (Rebesco et al., 2008, 2014), such as banks or seamounts (e.g., Martorelli et al., 2011; Vandorpe et al., 2014; Liu et al., 2019). However, the topography described herein does not display any obvious irregularity that might increase current velocity to produce such a deep-cutting channel. Additionally, the submarine fan system observed in the unit 1b in the MB is of Paleocene in age, which could be the corresponding depositional products transported through this conduit, thus further supporting an origin by turbidity current erosion (Stage B in Fig. 13).

In the subsequent period of channel filling, four stages are

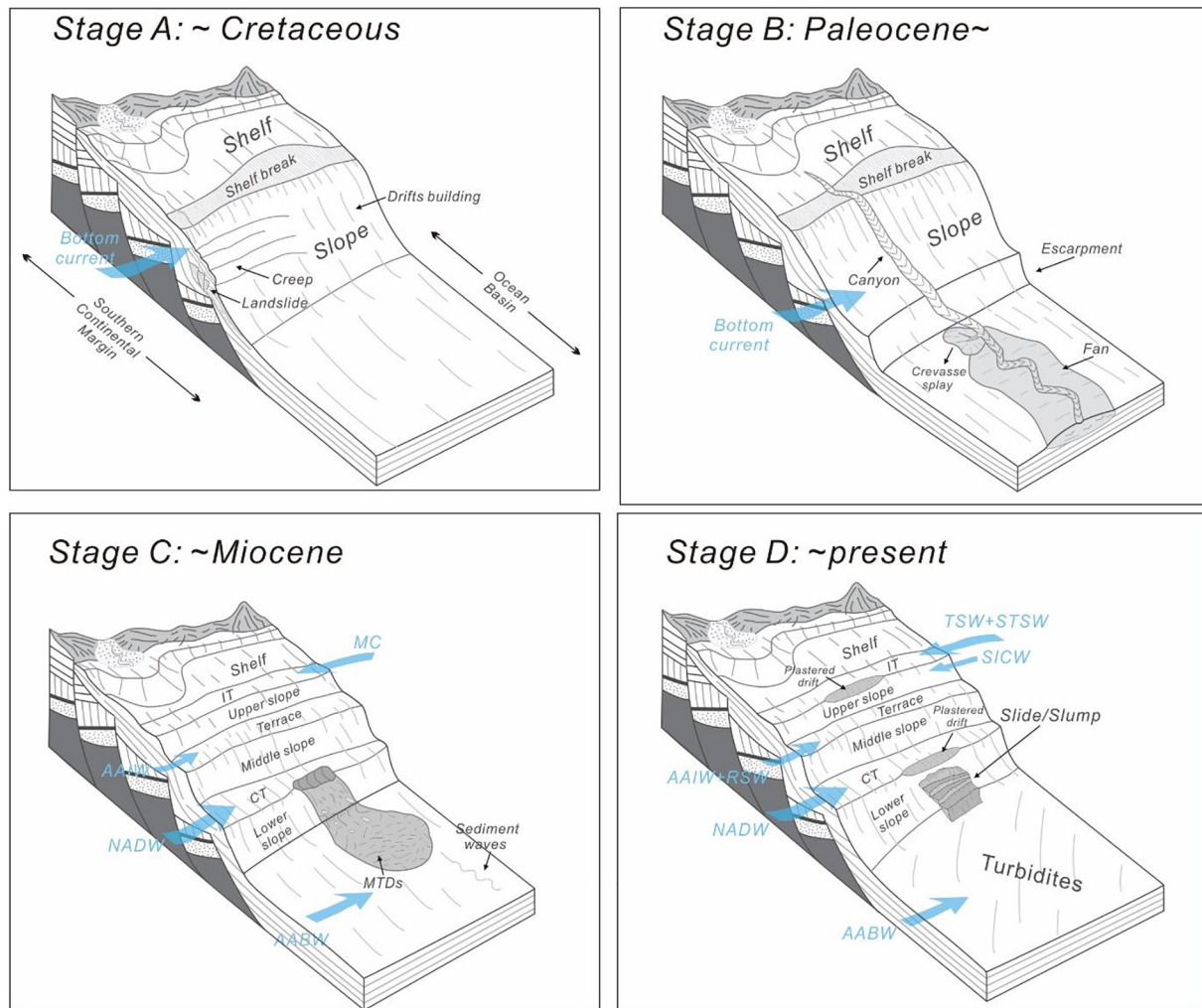


Fig. 13. Four-staged conceptual model interpreting the depositional evolution off the southern Mozambique margin. Referred from Dingle et al. (1978); Preu et al. (2011) and Miramontes et al. (2019). Abbreviation: IT = Inharrime Terrace; CT = Central Terrace; MC = Mozambique current; AAIW = Antarctic Intermediate Water; RSW = Red Sea Water; NADW = North Atlantic Deep Water; AABW = Antarctic Bottom Water; TSW = Tropical Surface Water; STSW = Sub-Tropical Surface Water; SICW = South Indian Central Water. (For interpretation of the references to colour in this figure legend, the reader is referred to the web version of this article.)

recognized bounded by erosional surfaces shown by the truncation of lateral reflections (illustrated by black dotted lines in Fig. 12). The depositional pattern in each stage is quite different. Facies in stage I are marked by a series of well-layered, continuous, strong amplitude and moderate-high frequency reflectors. The early part of stage II has oblique and medium amplitude reflectors that show a progradational pattern, downlapping on to the channel wall, with a dip of up to 20° towards the northwest. At the base of stage III deposition, upward clinoform-like deposits are observed in a set of horizontally arranged reflectors with strong amplitude and moderate frequency, indicating vertical aggradation, above which mounded sediments are observed, with the maximum height up to 0.1 s TWT. Deposition in stage IV is part of post-T1 sediments, as they have similar seismic characters of generally weak amplitude of reflectors. A group of parallel and well-layered reflectors becomes slightly wavy to the southeast, which is bounded above and below by sediments of chaotic to transparent seismic reflection pattern. Bottom currents can produce such laterally continuous deposits that act as prograding clinoform-like deposits within channels (Faugères et al., 1999; Mulder et al., 2008). Northwestward channel migration matches the prograding direction of clinoform-like deposits particularly, evidencing the effects of bottom current rather than purely turbidity channel migration (e.g., Viana et al., 1998; Faugères et al., 1999). Mounded sediments associated with

erosional incision are typical of CDS construction, according to seismo-stratigraphic criteria defined by Faugères et al. (1999), Rebesco and Stow (2001) and Stow (2002).

6.1.4. Sedimentary hiatus from the late Eocene to the early Miocene

Horizon T1 is partly an erosional surface, shown by truncated seismic reflection pattern and characterized by onlapping overlying reflectors. By comparison with the stratigraphic framework, we consider it is an unconformity that marks a sedimentary hiatus from at least the Oligocene to no later than early/middle Miocene. This can be attributed either to tectonic uplift and continental or shallow-water erosion/non-deposition, or to strong bottom-current scour and non-deposition in deeper water.

Along the Mozambique margin, Castellino et al. (2015) identified a prominent erosional unconformity during the mid-Oligocene in the north and considered it as the result of marine regression due to the fact that no major current controlled features were observed. Nevertheless, near the study area, Site 249 drilled on the MozR encountered the maximum duration of the Oligocene hiatus (from the late Cretaceous to the early/middle Miocene), indicating that the physical causes of the non-deposition/erosion ceased operating in the early/middle Miocene but could have been started at any earlier time. Sites 248 and 250 in the nearby MB contain the Oligocene hiatus, which also matches the

boundary t1 of strong amplitude and good continuity (Fig. 4). It suggests similar non-deposition/erosion process exists in both the continental margin and the MB. DSDP stratigraphic records throughout the Indian Ocean revealed that these unconformities or undated hiatuses occur at all water depths (Davies et al., 1975). Some hiatuses in the sediments of the south-west Indian Ocean seemingly correspond to tectonic events on land (Kent, 1974), but in many locations there is no clear case for a tectonic origin for the unconformities. We therefore interpret the hiatus associated with horizon T1 on the CT to be the result of enhanced bottom-current activity in relatively deep water.

The opening of the Drake Passage gateway (~35 Ma) allowed the establishment of the Antarctic Circumpolar Current (Martos et al., 2013), which is related to the development of a transition from an ice-free period to a time with large-scale ice build-up on Antarctica (Ehrmann, 1991; Miller et al., 1991; Ehrmann et al., 1992; Wise Jr et al., 1992). Numerous proxies have reflected this event, e.g., clay mineralogy on the Kerguelen Plateau (Ehrmann and Mackensen, 1992); a major shift in oxygen isotopes related to the early Oligocene glacier growth (Kennett and Stott, 1990; Barrera and Huber, 1993; Zachos et al., 1994); and an increase in productivity from the late Eocene to an early Oligocene productivity maximum in the Weddell Sea (Diester-Haass and Zahn, 1996). The onset of ice build-up as one of the major climatic changes associated with Antarctica thermal isolation at the Eocene-Oligocene boundary also had great impact on the oceanography of the Southern Hemisphere regions, especially intensification of the bottom currents. Evidence includes the strengthening of AABW documented by the broader dispersal of Antarctic particles into the Southern Ocean (Diester-Haass and Zahn, 1996) and the development of the Oribi Drift in the Natal Valley (Niemi et al., 2000). Thus, there is evidence from which we suggest that the onset of fast erosive currents following Antarctic glaciation and isolation could be applied to explain the widely-distributed sedimentary hiatus during this period. The presence of the moats (Fig. 4, CDPs 16209-17009 at 3.1–3.3 s TWT; CDPs 18,209–18,809 at 3.2–3.4 s TWT) further support this interpretation as they suggest faster bottom currents, in places further intensified by interaction with the topographic high (Fig. 4, CDPs 16209; 17809-18209 at 3.2–3.4 s TWT).

6.1.5. Along-slope processes dominated sedimentation since the Middle Miocene

The seismic characteristics of the CT area show a notable change with greatly weakened amplitudes from unit 3A to unit 4A, indicating a change sedimentation condition, perhaps in response to a cooling event in the middle Miocene (Zachos et al., 2001). This similar climate effect is widely recognized in the Indian Ocean and reflected by depositional pattern change at the Agulhas Ridge (Wildeboer Schut et al., 2002), in the Transkei Basin (Schlüter and Uenzelmann-Neben, 2007) and also in the nearby Natal Valley (Niemi et al., 2000). Evidence for a different current circulation regime in the study area is documented by the contourite terrace architecture associated with the re-establishment of a CDS in unit 4A.

NADW originating in Arctic regions flows through the Atlantic and passes the Agulhas Passage to enter into the MB (Van Aken et al., 2004). In the southwest Indian Ocean, proto-NADW has been inferred at least since middle Miocene times (Frank et al., 2002). In vertical profile, the NADW separates AAIW and AABW in the modern ocean (Fig. 2c). The initiation of NADW, therefore, probably resulted in a vertical re-arrangement of water masses and their associated interfaces. These morpho-sedimentary and hydrographic coincidences lead us to propose that following the onset of NADW in the region, water masses were re-established into a new circulation pattern (Stage C in Fig. 13), and the shifted interfaces would allow the build-up of a new CDS represented by seismic unit 4A. This hypothesis is further supported by the formation of the modern CT that coincides with the water depth range of the interface between AAIW and NADW. An earlier study (Preu et al., 2013) has revealed a distinct correlation between depths of the terraces and

the depths of the water mass interfaces and suggested turbulent, energetic current patterns driven by major vertical density gradients associated with these interface zones as initial mechanism for terrace genesis. A similar conclusion was reached by Preu et al. (2012), suggesting the change of oceanographic regime related to the shift of water mass boundaries has controlled the northern Argentine slope evolution and terrace development.

In the MB, extensive turbidites with varied amplitudes of reflectors characterise unit 3b. This is the consequence of the further expansion of the turbidite system off the Zambezi Delta since the Miocene (Stage D in Fig. 13). A major sediment flux has been identified and a large proportion of this sediment bypassed the shelf as well as the upper fan region through the Zambezi Valley system, and fed directly into the Mozambique Channel. Much of this material was deposited as turbidites across the MB (Wiles et al., 2017a, 2017b; Castellino et al., 2017; Miramontes et al., 2019; Fierens et al., 2019), which formed the distal lobe of the middle-lower fan in the study area.

6.2. The role of the MFZ and escarpment

The MFZ was created by a large transform fault related to a major offset in the SW Indian Ocean Ridge (Fig. 1a). In this area it is associated with a distinct roughly N-S trending escarpment, from the CT (i.e., shallow offshore continuation of the MCP in Fig. 1a, b) to the MozR at the eastern flank (Fig. 1b; Mueller et al., 2016; Baby et al., 2018). The elevation of the ridge is the result of enhanced magmatism, perhaps of large igneous province (LIP) origin (Fischer et al., 2016; Jacques et al., 2019), which may have contributed to the development of the prominent escarpment along the eastern flank of the MozR. It can be observed this escarpment extends further north, with a height up to 1500 m above the MB abyssal plain in the study area (Fig. 3).

From the studied seismic profile, compared to the MB, the CT has experienced a longer geological time of sedimentary evolution in the Cretaceous, with substantial sediment supply along the margin (Walford et al., 2005; Said et al., 2015). During this period, the onset of bottom current activity led to the erosion, transport and deposition of contourite material, allowing for significant sediment accumulation, as the identified drifts in Fig. 11. This is concordant with the observation from the Argentine and Uruguayan margin, where the contourite terraces are associated with a steep escarpment of more than 1000 m in height (Preu et al., 2013; Hernández-Molina et al., 2016). Therefore, a sedimentary role in the development of this escarpment cannot be ruled out.

The MFZ and its associated escarpment have played an important role on deposition of the study area. On the one hand, this local steep slope can promote down-slope processes, e.g., the Paleocene fan system below t2 on the MB; MTDs and slide/slump transport. On the other hand, the existing height difference acts as a barrier, limiting the turbidites supplied from Zambezi River to within the MB, while the CT between 1900–2300 m water depth was exposed to relatively strong hydrodynamic conditions and bottom-current activity leading to development of a new CDS. In this way, the MFZ has greatly influenced deposition since the middle Miocene.

7. Conclusions

On the basis of the seismic architecture identified in the study area and the associated seismic facies, four major units within the Central Terrace and three units in the Mozambique Basin are distinguished on seismic data. The ages of the boundaries could be defined by linking the architecture of the units to the regionally established stratigraphy. A complex deep-water sedimentary system has been developed, which comprises downslope architectural elements – slides/slumps, slope creep, canyon incision, MTDs, and submarine fan deposition – as well as alongslope architectural elements and evolution of a contourite depositional system related to bottom currents activity.

The initiation of vigorous bottom-water circulation on the studied continental slope (Central Terrace) can be dated back to the Late Cretaceous, a period when sedimentation was controlled by current action. Bottom current activity and flow velocity varied through geological time. During the Paleocene-Eocene, less bottom current activity is reflected by widespread sheeted drifts. In the Late Eocene, the Antarctic isolation was most likely responsible for the generation of more intense bottom currents from the top of unit 3A in the study area, which further led to the Oligocene sedimentary hiatus. By the Middle Miocene, a new water-mass circulation pattern was established, forming a new contourite depositional system in unit 4A and building up a contourite terrace at the interface between water masses. Whereas the major escarpment associated with the MFZ is most likely due to enhanced magmatism during the Cretaceous, it has since been sculpted by both downslope and alongslope processes. Its presence has also exerted significant influence on deposition locally.

In summary, the present study has evidenced the initiation and evolution of bottom water circulation, the nature of diverse gravitational deposits, and how these alongslope and downslope processes have jointly taken part in the construction and shaping of the southern Mozambique margin.

Declaration of competing interest

The authors declare that they have no known competing financial interests or personal relationships that could have appeared to influence the work reported in this paper.

Acknowledgements

The study was supported by the National Natural Science Foundation of China (Nos. 41830537, 41476048), the National Key Research and Development Program of China (No. 2017YFC1405504) and the Fundamental Research Funds for National Universities, China University of Geosciences (Wuhan). DS acknowledges support from his position as Distinguished Professor at the China University of Geosciences, Wuhan. We thank Ben Kneller and Calvin Campbell for their fruitful comments and suggestions. We also thank two anonymous reviewers and guest editor Wilfried Jokat for providing many helpful comments and suggestions, which significantly improved the manuscript.

References

- Alves, T.M., 2015. Submarine slide blocks and associated soft-sediment deformation in deep-water basins: a review. *Mar. Pet. Geol.* 67, 262–285.
- Baby, G., Guillocheau, F., Boulogne, C., Robin, C., Dall'Asta, M., 2018. Uplift history of a transform continental margin revealed by the stratigraphic record: the case of the Agulhas transform margin along the Southern African Plateau. *Tectonophysics* 731, 104–130.
- Barrera, E., Huber, B.T., 1993. Eocene to Oligocene oceanography and temperatures in the Antarctic Indian Ocean. The Antarctic paleoenvironment: A perspective on global change: American Geophysical Union Antarctic Research Series 60, 49–65. <https://doi.org/10.1029/AR060p0049>.
- Ben-Avraham, Z., Niemi, T.M., Hartnady, C.J., 1994. Mid-Tertiary changes in deep ocean circulation patterns in the Natal Valley and Transkei Basin, Southwest Indian Ocean. *Earth Planet. Sci. Lett.* 121, 639–646.
- Bianchi, G., McCave, I., 2000. Hydrography and sedimentation under the deep western boundary current on Björn and Gardar Drifts, Iceland Basin. *Mar. Geol.* 165, 137–169.
- Boyer, T.P., Baranova, O.K., Coleman, C., Garcia, H.E., Grodsky, A., Locarnini, R.A., Mishonov, A.V., Paver, C.R., Reagan, J.R., Seidov, D., Smolyar, I.V., Weathers, K.W., Zweng, M.M., 2019. World Ocean Database 2018. A. V. Mishonov, Technical Editor, NOAA Atlas NESDIS 87.
- Bull, S., Cartwright, J., Huuse, M., 2009. A review of kinematic indicators from mass-transport complexes using 3D seismic data. *Mar. Pet. Geol.* 26, 1132–1151.
- Castelino, J.A., Reichert, C., Klingelhoefer, F., Aslanian, D., Jokat, W., 2015. Mesozoic and Early Cenozoic sediment influx and morphology of the Mozambique Basin. *Mar. Pet. Geol.* 66, 890–905.
- Castelino, J.A., Eagles, G., Jokat, W., 2016. Anomalous bathymetry and palaeobathymetric models of the Mozambique Basin and Riiser Larsen Sea. *Earth Planet. Sci. Lett.* 455, 25–37.
- Castelino, J.A., Reichert, C., Jokat, W., 2017. Response of Cenozoic turbidite system to tectonic activity and sea-level change off the Zambezi Delta. *Mar. Geophys. Res.* 38, 209–226.
- Coffin, M.F., Rabinowitz, P.D., Houtz, R.E., 1986. Crustal structure in the western Somali Basin. *Geophys. J. Int.* 86, 331–369.
- Davies, T.A., Weser, O.E., Luyendyk, B.P., Kidd, R.B., 1975. Unconformities in the sediments of the Indian Ocean. *Nature* 253, 15.
- De Ruijter, W.P., Ridderinkhof, H., Lutjeharms, J.R., Schouten, M.W., Veth, C., 2002. Observations of the flow in the Mozambique Channel. *Geophys. Res. Lett.* 29, 140–141.
- Deptuck, M.E., Steffens, G.S., Barton, M., Pirmez, C., 2003. Architecture and evolution of upper fan channel-belts on the Niger Delta slope and in the Arabian Sea. *Mar. Pet. Geol.* 20, 649e676.
- Diester-Haass, L., Zahn, R., 1996. Eocene-Oligocene transition in the Southern Ocean: history of water mass circulation and biological productivity. *Geology* 24, 163–166.
- DiMarco, S.F., Chapman, P., Nowlin Jr., W.D., Hacker, P., Donohue, K., Luther, M., Johnson, G.C., Toole, J., 2002. Volume transport and property distributions of the Mozambique Channel. *Deep-Sea Res. II Top. Stud. Oceanogr.* 49, 1481–1511.
- Dingle, R., Goodlad, S., Martin, A., 1978. Bathymetry and stratigraphy of the northern Natal Valley (SW Indian Ocean): a preliminary account. *Mar. Geol.* 28, 89–106.
- Du Toit, S.R., Leith, M.J., 1974. The J (c)-1 bore-hole on the continental shelf near Stanger, Natal. *S. Afr. J. Geol.* 77, 247–252.
- Eagles, G., König, M., 2008. A model of plate kinematics in Gondwana breakup. *Geophys. J. Int.* 173, 703–717.
- Ehrmann, W., 1991. Implications of Sediment Composition on the Southern Kerguelen Plateau for Paleoclimate and Depositional Environment. Presented at the Proceedings of the Ocean Drilling Program, Scientific Results, College Station, pp. 185–210. <https://doi.org/10.2973/odp.proc.sr.119.121.1991>.
- Ehrmann, W.U., Mackensen, A., 1992. Sedimentological evidence for the formation of an East Antarctic ice sheet in Eocene/Oligocene time. *Palaeogeogr. Palaeoclimatol. Palaeoecol.* 93, 85–112. <https://doi.org/10.1029/GM070p0423>.
- Ehrmann, W., Hambrey, M., Baldauf, J., Barron, J., Larsen, B., Mackensen, A., Wise Jr., S., Zachos, J., 1992. History of Antarctic glaciation: an Indian Ocean perspective. Washington DC American Geophysical Union Geophysical Monograph Series 70, 423–446.
- Elliott, G.M., Parson, L.M., 2008. Influence of sediment drift accumulation on the passage of gravity-driven sediment flows in the Iceland Basin, NE Atlantic. *Mar. Pet. Geol.* 25, 219–233.
- Ercilla, G., Alonso, B., Estrada, F., Chiocci, F.L., Baraza, J., Farran, M., 2002. The Magdalena Turbidite System (Caribbean Sea): present-day morphology and architecture model. *Mar. Geol.* 185, 303–318. [https://doi.org/10.1016/S0025-3227\(02\)00182-2](https://doi.org/10.1016/S0025-3227(02)00182-2).
- Faugères, J.-C., Stow, D., 2008. Contourite drifts: nature, evolution and controls. *Dev. Sedimentol.* 60, 257–288. [https://doi.org/10.1016/S0070-4571\(08\)10014-0](https://doi.org/10.1016/S0070-4571(08)10014-0).
- Faugères, J.-C., Stow, D.A., Imbert, P., Viana, A., 1999. Seismic features diagnostic of contourite drifts. *Mar. Geol.* 162, 1–38.
- Faugères, J.-C., Gonthier, E., Mulder, T., Kenyon, N., Cirac, P., Grimbold, R., Berne, S., Lesuave, R., 2002. Multi-process generated sediment waves on the Landes Plateau (Bay of Biscay, North Atlantic). *Mar. Geol.* 182, 279–302.
- Fierens, R., Droz, L., Toucanne, S., Raison, F., Jouet, G., Babonneau, N., Miramontes, E., Landurain, S., Jorry, S.J., 2019. Late Quaternary geomorphology and sedimentary processes in the Zambezi turbidite system (Mozambique Channel). *Geomorphology* 334, 1–28.
- Fischer, M.D., Uenzelmann-Neben, G., 2018. Late Cretaceous onset of current controlled sedimentation in the African–Southern Ocean gateway. *Mar. Geol.* 395, 380–396.
- Fischer, M.D., Uenzelmann-Neben, G., Jacques, G., Werner, R., 2016. The Mozambique Ridge: a document of massive multi-stage magmatism. *Geophys. J. Int.* 208, 449–467.
- Flood, R.D., Piper, D.J., 1997. Amazon Fan Sedimentation: The Relationship to Equatorial Climate Change, Continental Denudation, and Sea-Level Fluctuations. Presented at the Proceedings-ocean Drilling Program Scientific Results, National Science Foundation, pp. 653–675. <https://doi.org/10.2973/odp.proc.sr.155.246.1997>.
- Flores, G., 1973. The Cretaceous and Tertiary sedimentary basins of Mozambique and Zululand. *Sedimentary Basins of the African Coasts* 2, 81–111.
- Frank, M., Whiteley, N., Kasten, S., Hein, J.R., O'Nions, K., 2002. North Atlantic Deep Water export to the Southern Ocean over the past 14 Myr: evidence from Nd and Pb isotopes in ferromanganese crusts. *Paleoceanography* 17, 1–12.
- Girdley, W., 1974. Lithologic summary, Leg 25, Deep Sea Drilling Project. DSDP Init Repts 25, 725–741.
- Gong, C., Wang, Y., Zhu, W., Li, W., Xu, Q., 2013. Upper Miocene to Quaternary unidirectionally migrating deep-water channels in the Pearl River mouth Basin, northern South China Sea. *AAPG Bull.* 97, 285–308.
- Habgood, E.L., Kenyon, N.H., Masson, D.G., Akhmetzhanov, A., Weaver, P.P., Gardner, J., Mulder, T., 2003. Deep-water sediment wave fields, bottom current sand channels and gravity flow channel-lobe systems: Gulf of Cadiz, NE Atlantic. *Sedimentology* 50, 483–510.
- Hanquiez, V., Mulder, T., Toucanne, S., Lecroart, P., Bonnel, C., Marchès, E., Gonthier, E., 2010. The sandy channel-lobe depositional systems in the Gulf of Cadiz: gravity processes forced by contour current processes. *Sediment. Geol.* 229, 110–123.
- Hanyu, T., Nogi, Y., Fujii, M., 2017. Crustal formation and evolution processes in the Natal Valley and Mozambique Ridge, off South Africa. *Polar Science* 13, 66–81.
- He, Y., Xie, X., Kneller, B.C., Wang, Z., Li, X., 2013. Architecture and controlling factors of canyon fills on the shelf margin in the Qiongdongnan Basin, northern South China Sea. *Mar. Pet. Geol.* 41, 264–276.
- He, Y., Zhong, G., Wang, L., Kuang, Z., 2014. Characteristics and occurrence of submarine canyon-associated landslides in the middle of the northern continental slope, South China Sea. *Mar. Pet. Geol.* 57, 546–560.

- Hernández-Molina, F., Larter, R., Rebesco, M., Maldonado, A., 2006. Miocene reversal of bottom water flow along the Pacific Margin of the Antarctic Peninsula: stratigraphic evidence from a contourite sedimentary tail. *Mar. Geol.* 228, 93–116.
- Hernández-Molina, F.J., Llave, E., Stow, D.A.V., 2008. Chapter 19 continental slope contourites. In: Rebesco, M., Camerlenghi, A. (Eds.), *Contourites. Developments in Sedimentology*, vol. 60. Elsevier, Amsterdam, pp. 379–408.
- Hernández-Molina, F., Paterlini, M., Somoza, L., Violante, R., Arecco, M., De Isasi, M., Rebesco, M., Uenzelmann-Neben, G., Neben, S., Marshall, P., 2010. Giant mounded drifts in the Argentine Continental Margin: origins, and global implications for the history of thermohaline circulation. *Mar. Pet. Geol.* 27, 1508–1530.
- Hernández-Molina, F.J., Soto, M., Piola, A.R., Tomasini, J., Preu, B., Thompson, P., Badalini, G., Creaser, A., Violante, R.A., Morales, E., 2016. A contourite depositional system along the Uruguayan continental margin: sedimentary, oceanographic and paleoceanographic implications. *Mar. Geol.* 378, 333–349.
- Hodgson, D.M., Flint, S.S., Hodgetts, D., Drinkwater, N.J., Johannessen, E.P., Luthi, S.M., 2006. Stratigraphic evolution of fine-grained submarine fan systems, Tanqua depocenter, Karoo Basin, South Africa. *J. Sediment. Res.* 76, 20–40.
- Hodgson, D.M., Kane, I.A., Flint, S.S., Brunt, R.L., Ortiz-Karpp, A., 2016. Time-transgressive confinement on the slope and the progradation of basin-floor fans: implications for the sequence stratigraphy of deep-water deposits. *J. Sediment. Res.* 86, 73–86.
- Huang, Y., Yao, G., Fan, X., 2019. Sedimentary characteristics of shallow-marine fans of the Huangliu Formation in the Yinggehai Basin, China. *Mar. Pet. Geol.* 110, 403–419.
- Izumi, K., Miyaji, T., Tanabe, K., 2012. Early Toarcian (Early Jurassic) oceanic anoxic event recorded in the shelf deposits in the northwestern Panthalassa: evidence from the Nishinakayama Formation in the Toyora area, west Japan. *Palaeogeogr. Palaeoclimatol. Palaeoecol.* 315, 100–108.
- Jacques, G., Hauff, F., Hoernle, K., Werner, R., Uenzelmann-Neben, G., Garbe-Schönberg, D., Fischer, M., 2019. Nature and origin of the Mozambique Ridge, SW Indian Ocean. *Chem. Geol.* 507, 9–22.
- Jokat, W., Boebel, T., König, M., Meyer, U., 2003. Timing and geometry of early Gondwana breakup. *Journal of Geophysical Research: Solid Earth* 108.
- Jones, G.D., 1982. *Euxinic. Beaches and Coastal Geology* 420–421. https://doi.org/10.1007/0-387-30843-1_181.
- Kennett, J.P., Stott, L., 1990. Proteus and Proto-Oceanus: Ancestral Paleogene Oceans as Revealed from Antarctic Stable Isotopic Results; ODP Leg 113. Presented at the Proceedings of the Ocean Drilling Program, Scientific Results, Ocean Drilling Program College Station, Tex, pp. 865–880.
- Kent, P., 1974. Continental Margin of East Africa—a Region of Vertical Movements, in: *The Geology of Continental Margins*. Springer, pp. 313–320. https://doi.org/10.1007/978-3-662-01141-6_23.
- Kneller, B., Buckee, C., 2000. The structure and fluid mechanics of turbidity currents: a review of some recent studies and their geological implications. *Sedimentology* 47, 62–94. <https://doi.org/10.1046/j.1365-3091.2000.047s1062.x>.
- Kneller, B., Dykstra, M., Fairweather, L., Milana, J.P., 2016. Mass-transport and slope accommodation: implications for turbidite sandstone reservoirs. *AAPG Bull.* 100, 213–235.
- Kolla, V., Sullivan, L., Streeter, S.S., Langseth, M.G., 1976. Spreading of Antarctic Bottom Water and its effects on the floor of the Indian Ocean inferred from bottom-water potential temperature, turbidity, and sea-floor photography. *Mar. Geol.* 21, 171–189.
- Kolla, V., Eittreim, S., Sullivan, L., Kosteki, J.A., Burckle, L.H., 1980. Current-controlled, abyssal microtopography and sedimentation in Mozambique Basin, southwest Indian Ocean. *Mar. Geol.* 34, 171–206.
- König, M., Jokat, W., 2010. Advanced insights into magmatism and volcanism of the Mozambique Ridge and Mozambique Basin in the view of new potential field data. *Geophys. J. Int.* 180, 158–180.
- Lawver, L.A., Gahagan, L.M., Coffin, M.F., 1992. The development of paleoseaways around Antarctica. *Antarctic Research Series* 56, 7–30.
- Lee, S., Chough, S., 2001. High-resolution (2–7 kHz) acoustic and geometric characters of submarine creep deposits in the South Korea Plateau, East Sea. *Sedimentology* 48, 629–644.
- Lee, H.J., Syvitski, J.P., Parker, G., Orange, D., Locat, J., Hutton, E.W., Imran, J., 2002. Distinguishing sediment waves from slope failure deposits: field examples, including the ‘Humboldt slide’, and modelling results. *Mar. Geol.* 192, 79–104.
- Leinweber, V.T., Jokat, W., 2012. The Jurassic history of the Africa–Antarctica corridor—new constraints from magnetic data on the conjugate continental margins. *Tectonophysics* 530, 87–101.
- Liu, S., Van Rooij, D., Vandorpe, T., González-Pola, C., Ercilla, G., Hernández-Molina, F.J., 2019. Morphological Features and Associated Bottom-Current Dynamics in the Le Danois Bank Region (Southern Bay of Biscay, NE Atlantic): A Model in a Topographically Constrained Small Basin. *Deep Sea Research Part I, Oceanographic Research Papers*.
- Llave, E., Hernández-Molina, F., Somoza, L., Díaz-del-Río, V., Stow, D., Maestro, A., Dias, J.A., 2001. Seismic stacking pattern of the Faro-Albufeira contourite system (Gulf of Cadiz): a Quaternary record of paleoceanographic and tectonic influences. *Mar. Geophys. Res.* 22, 487–508.
- Llave, E., Schönfeld, J., Hernández-Molina, F., Mulder, T., Somoza, L., Del Río, V.D., Sánchez-Almazo, I., 2006. High-resolution stratigraphy of the Mediterranean outflow contourite system in the Gulf of Cadiz during the late Pleistocene: the impact of Heinrich events. *Mar. Geol.* 227, 241–262.
- Locat, J., Lee, H.J., 2002. Submarine landslides: advances and challenges. *Can. Geotech. J.* 39, 193–212.
- Lutjeharms, J.R., 2006. *The Agulhas Current*. 329 pp. <https://doi.org/10.1007/3-540-37212-1>.
- Marchès, E., Mulder, T., Gonthier, E., Cremer, M., Hanquiez, V., Garlan, T., Lecroart, P., 2010. Perched lobe formation in the Gulf of Cadiz: interactions between gravity processes and contour currents (Algarve Margin, Southern Portugal). *Sediment. Geol.* 229, 81–94.
- Martin, A.K., 1981. The influence of the Agulhas Current on the physiographic development of the northernmost Natal Valley (S.W. Indian Ocean). *Mar. Geol.* 39, 259–276. [https://doi.org/10.1016/0025-3227\(81\)90075-X](https://doi.org/10.1016/0025-3227(81)90075-X).
- Martin, A., Goodlad, S., Salmon, D., 1982. Sedimentary basin in-fill in the northernmost Natal Valley, hiatus development and Agulhas Current palaeo-oceanography. *J. Geol. Soc.* 139, 183–201.
- Martorelli, E., Petroni, G., Chiocci, F.L., 2011. Contourites offshore Pantelleria Island (Sicily Channel, Mediterranean Sea): depositional, erosional and biogenic elements. *Geo-Mar. Lett.* 31, 481–493.
- Martos, Y.M., Maldonado, A., Lobo, F.J., Hernández-Molina, F.J., Pérez, L.F., 2013. Tectonics and paleoceanographic evolution recorded by contourite features in southern Drake Passage (Antarctica). *Mar. Geol.* 343, 76–91.
- Massuanganhe, E.A., Westerberg, L.-O., Risberg, J., 2018. Morphodynamics of deltaic wetlands and implications for coastal ecosystems—a case study of Save River Delta, Mozambique. *Geomorphology* 322, 107–116.
- Mayall, M., Jones, E., Casey, M., 2006. Turbidite channel reservoirs—Key elements in facies prediction and effective development. *Mar. Pet. Geol.* 23, 821–841. <https://doi.org/10.1016/j.marpetgeo.2006.08.001>.
- Meyers, P.A., 2006. Paleoclimatic and paleoceanographic similarities between Mediterranean sapropels and Cretaceous black shales. *Palaeogeogr. Palaeoclimatol. Palaeoecol.* 235, 305–320.
- Miller, K.G., Wright, J.D., Fairbanks, R.G., 1991. Unlocking the icehouse: Oligocene to Miocene oxygen isotope, eustasy and marginal erosion. *J. Geophys. Res.* 96, 6829–6848.
- Miramontes, E., Penven, P., Fierens, R., Droz, L., Toucanne, S., Jorry, S.J., Jouet, G., Pastor, L., Jacinto, R.S., Gaillot, A., 2019. The influence of bottom currents on the Zambezi Valley morphology (Mozambique Channel, SW Indian Ocean): in situ current observations and hydrodynamic modelling. *Mar. Geol.* 410, 42–55.
- Moscardelli, L., Wood, L., Mann, P., 2006. Mass-transport complexes and associated processes in the offshore area of Trinidad and Venezuela. *AAPG Bull.* 90, 1059–1088.
- Mueller, C.O., Jokat, W., 2017. Geophysical evidence for the crustal variation and distribution of magmatism along the central coast of Mozambique. *Tectonophysics* 712–713, 684–703.
- Mueller, C.O., Jokat, W., 2019. The initial Gondwana break-up: a synthesis based on new potential field data of the Africa–Antarctica Corridor. *Tectonophysics* 750, 301–328. <https://doi.org/10.1016/j.tecto.2018.11.008>.
- Mueller, C.O., Jokat, W., Schreckenberger, B., 2016. The crustal structure of Beira High, central Mozambique—combined investigation of wide-angle seismic and potential field data. *Tectonophysics* 683, 233–254.
- Mulder, T., Etienne, S., 2010. Lobes in deep-sea turbidite systems: state of the art. *Sediment. Geol.* 3, 75–80.
- Mulder, T., Faugères, J.-C., Gonthier, E., 2008. Mixed turbidite–contourite systems. *Dev. Sedimentol.* 60, 435–456.
- Mulder, T., Hüneke, H., Van Loon, A., 2011. Progress in deep-sea sedimentology. In: *Developments in Sedimentology*. Elsevier, pp. 1–24. <https://doi.org/10.1016/B978-0-444-53000-4.00001-9>.
- Mutti, E., 1977. Distinctive thin-bedded turbidite facies and related depositional environments in the Eocene Hecho Group (South-central Pyrenees, Spain). *Sedimentology* 24, 107–131.
- Nairn, A.E., Lerche, I., Iliffe, J.E., 1991. Geology, basin analysis, and hydrocarbon potential of Mozambique and the Mozambique Channel. *Earth Sci. Rev.* 30, 81–123.
- Niemi, T.M., Ben-Avraham, Z., Hartnady, C.J., Reznikov, M., 2000. Post-Eocene seismic stratigraphy of the deep ocean basin adjacent to the southeast African continental margin: a record of geostrophic bottom current systems. *Mar. Geol.* 162, 237–258.
- Normark, W.R., 1970. Growth patterns of deep-sea fans. *AAPG Bull.* 54, 2170–2195. <https://doi.org/10.1306/5D25CC79-16C1-11D7-8645000102C1865D>.
- Normark, W.R., 1978. Fan valleys, channels, and depositional lobes on modern submarine fans: characters for recognition of sandy turbidite environments. *AAPG Bull.* 62, 912–931. <https://doi.org/10.1306/c1ea4f72-16c9-11d7-8645000102c1865d>.
- Normark, W.R., Hess, G.R., Stow, D., Bowen, A., 1980. Sediment waves on the Monterey Fan levee: a preliminary physical interpretation. *Mar. Geol.* 37, 1–18.
- Pickering, K., Hiscott, R., 2016. *Deep Marine Systems. Processes, Deposits, Environments, Tectonics and Sedimentation*. 657 pp.. AGU and Wiley.
- Piper, D.J., Normark, W.R., 2009. Processes that initiate turbidity currents and their influence on turbidites: a marine geology perspective. *J. Sediment. Res.* 79, 347–362.
- Preu, B., Spieß, V., Schwenk, T., Schneider, R., 2011. Evidence for current-controlled sedimentation along the southern Mozambique continental margin since Early Miocene times. *Geo-Mar. Lett.* 31, 427–435.
- Preu, B., Schwenk, T., Hernández-Molina, F.J., Violante, R., Paterlini, M., Krastel, S., Tomasini, J., Spieß, V., 2012. Sedimentary growth pattern on the northern Argentine slope: the impact of North Atlantic Deep Water on southern hemisphere slope architecture. *Mar. Geol.* 329, 113–125.
- Preu, B., Hernández-Molina, F.J., Violante, R., Piola, A.R., Paterlini, C.M., Schwenk, T., Voigt, I., Krastel, S., Spiess, V., 2013. Morphosedimentary and hydrographic features of the northern Argentine margin: the interplay between erosive, depositional and gravitational processes and its conceptual implications. *Deep-Sea Res. I Oceanogr. Res. Pap.* 75, 157–174.
- Quadfasel, D.R., 2001. Red Sea circulation. In: *Encyclopedia of Ocean Sciences*. Academic Press, pp. 2366–2376. <https://doi.org/10.1016/B978-0-12-813081-0.00377-3>.
- Quarty, G., de Cuevas, B., Coward, A., 2013. Mozambique Channel eddies in GCMs: a question of resolution and slippage. *Ocean Model.* 63, 56–67.
- Quilty, P.G., 2011. Late Jurassic foraminifera, Wallaby Plateau, offshore Western Australia. *The Journal of Foraminiferal Research* 41, 182–195.
- Rebesco, M., Camerlenghi, A., 2008. Contourites. *Developments in Sedimentology*.

- Developments in Sedimentology 60, 663.
- Rebesco, M., Stow, D., 2001. Seismic expression of contourites and related deposits: a preface. *Mar. Geophys. Res.* 22, 303–308.
- Rebesco, M., Camerlenghi, A., Van Loon, A., 2008. Contourite research: a field in full development. *Dev. Sedimentol.* 60, 1–10.
- Rebesco, M., Hernández-Molina, F.J., Van Rooij, D., Wählin, A., 2014. Contourites and associated sediments controlled by deep-water circulation processes: state-of-the-art and future considerations. *Mar. Geol.* 352, 111–154.
- Reeves, C., 2000. The geophysical mapping of Mesozoic dyke swarms in southern Africa and their origin in the disruption of Gondwana. *J. Afr. Earth Sci.* 30, 499–513.
- Revil, A., Grauls, D., Brévar, O., 2002. Mechanical compaction of sand/clay mixtures. *Journal of Geophysical Research: Solid Earth* 107https://doi.org/10.1029/2001JB000318 C. (ECV-11).
- Said, A., Moder, C., Clark, S., Ghorbal, B., 2015. Cretaceous–Cenozoic sedimentary budgets of the Southern Mozambique Basin: implications for uplift history of the South African Plateau. *J. Afr. Earth Sci.* 109, 1–10.
- Salman, G., Abdula, I., 1995. Development of the Mozambique and Rovuma sedimentary basins, offshore Mozambique. *Sediment. Geol.* 96, 7–41.
- Schlich, R., 1974. Sea-floor spreading history and deep-sea drilling results in the Madagascar and Mascarene Basins, western Indian Ocean. *Initial Rep. Deep Sea Drill. Proj.* 25, 663–678.
- Schlüter, P., Uenzelmann-Neben, G., 2007. Seismostratigraphic analysis of the Transkei Basin: a history of deep sea current controlled sedimentation. *Mar. Geol.* 240, 99–111.
- Schlüter, P., Uenzelmann-Neben, G., 2008. Indications for bottom current activity since Eocene times: the climate and ocean gateway archive of the Transkei Basin, South Africa. *Glob. Planet. Chang.* 60, 416–428.
- Schouten, M.W., de Ruijter, W.P., Van Leeuwen, P.J., Ridderinkhof, H., 2003. Eddies and variability in the Mozambique Channel. *Deep-Sea Res. II Top. Stud. Oceanogr.* 50, 1987–2003.
- Schwenk, T., Spiess, V., Breitzke, M., Hubscher, C., 2005. The architecture and evolution of the Middle Bengal Fan in vicinity of the active channel-levee system imaged by high-resolution seismic data. *Mar. Pet. Geol.* 22, 637–656.
- Senkans, A., Leroy, S., d'Acremont, E., Castilla, R., Despinois, F., 2019. Polyphase rifting and break-up of the central Mozambique margin. *Mar. Pet. Geol.* 100, 412–433.
- Simpson, E., Schlich, R., Gieskes, J., Girdley, W., Leclaire, L., Marshall, B., Moore, C., Muller, C., Sigal, J., Vallier, T., 1974. Site 249. *Init. Rep. Deep Sea Drill. Proj.* 25, 287–348.
- Steel, R., Olsen, T., Armentrout, J., Rosen, N., 2002. Clinoforms, clinoform trajectories and deepwater sands. In: Presented at the Sequence-Stratigraphic Models for Exploration and Production: Evolving Methodology, Emerging Models and Application Histories: Gulf Coast Section SEPM 22nd Research Conference, Houston, Texas, pp. 367–381. https://doi.org/10.5724/gcs.02.22.0367.
- Stow, D.A., 2002. Deep-water contourite systems: modern drifts and ancient series, seismic and sedimentary characteristics. *Geological Society of London.* https://doi.org/10.1144/GSL.MEM.2002.022.
- Stow, D.A., Mayall, M., 2000. Deep-water sedimentary systems: new models for the 21st century. *Mar. Pet. Geol.* 17, 125–135.
- Stow, D., Smillie, Z., 2020. Distinguishing between deep-water sediment facies: turbidites, contourites and hemipelagites. *Geosciences* 10, 68.
- Stow, D., Hunter, S., Wilkinson, D., Hernández-Molina, F., 2008. The nature of contourite deposition. *Dev. Sedimentol.* 60, 143–156.
- Stow, D.A., Hernández-Molina, F.J., Llave, E., Sayago-Gil, M., Díaz del Río, V., Branson, A., 2009. Bedform-velocity matrix: the estimation of bottom current velocity from bedform observations. *Geology* 37, 327–330.
- Stow, D., Hernández-Molina, F., Llave, E., Bruno, M., García, M., del Río, V.D., Somoza, L., Brackenkridge, R., 2013. The Cadiz Contourite Channel: sandy contourites, bedforms and dynamic current interaction. *Mar. Geol.* 343, 99–114.
- Sultan, N., Cochon, P., Foucher, J.-P., Mienert, J., 2004. Effect of gas hydrates melting on seafloor slope instability. *Mar. Geol.* 213, 379–401.
- Sun, Q., Xie, X., Piper, D.J., Wu, J., Wu, S., 2017a. Three dimensional seismic anatomy of multi-stage mass transport deposits in the Pearl River Mouth Basin, northern South China Sea: their ages and kinematics. *Mar. Geol.* 393, 93–108.
- Sun, Q., Alves, T., Xie, X., He, J., Li, W., Ni, X., 2017b. Free gas accumulations in basal shear zones of mass-transport deposits (Pearl River Mouth Basin, South China Sea): an important geohazard on continental slope basins. *Mar. Pet. Geol.* 81, 17–32.
- Symons, W.O., Sumner, E.J., Talling, P.J., Cartigny, M.J., Clare, M.A., 2016. Large-scale sediment waves and scours on the modern seafloor and their implications for the prevalence of supercritical flows. *Mar. Geol.* 371, 130–148.
- Thiéblemont, A., Hernández-Molina, F.J., Miramontes, E., Raison, F., Penven, P., 2019. Contourite depositional systems along the Mozambique channel: the interplay between bottom currents and sedimentary processes. *Deep-Sea Res. I Oceanogr. Res. Pap.* 147, 79–99.
- Toole, J.M., Warren, B.A., 1993. A hydrographic section across the subtropical South Indian Ocean. *Deep-Sea Res. I Oceanogr. Res. Pap.* 40, 1973–2019.
- Uenzelmann-Neben, G., 2002. Contourites on the Agulhas plateau, SW Indian Ocean: indications for the evolution of currents since Palaeogene times. *Geol. Soc. Lond. Mem.* 22, 271–288.
- Ullgren, J., van Aken, H., Ridderinkhof, H., De Ruijter, W., 2012. The hydrography of the Mozambique Channel from six years of continuous temperature, salinity, and velocity observations. *Deep-Sea Res. I Oceanogr. Res. Pap.* 69, 36–50.
- Ustinova, M., Tesakova, E., 2017. New data on microbiota of the Middle Volgian substage in the Loino Section (Kirov oblast). *Stratigr. Geol. Correl.* 25, 296–306.
- Vallier, T.L., Kidd, R.B., 1977. Volcanogenic sediments in the Indian Ocean. *Indian Ocean Geology and Biostratigraphy: Washington (Am. Geophys. Union)* 87–118. https://doi.org/10.1029/SP009p0087.
- Van Aken, H.M., Ridderinkhof, H., de Ruijter, W.P., 2004. North Atlantic deep water in the south-western Indian Ocean. *Deep-Sea Res. I Oceanogr. Res. Pap.* 51, 755–776.
- Van Rooij, D., Blamart, D., Kozachenko, M., Henriot, J.-P., 2007. Small mounded contourite drifts associated with deep-water coral banks, Porcupine Seabight, NE Atlantic Ocean. *Geol. Soc. Lond., Spec. Publ.* 276, 225–244.
- Vandorpe, T., Van Rooij, D., De Haas, H., 2014. Stratigraphy and paleoceanography of a topography-controlled contourite drift in the Pen Duick area, southern Gulf of Cádiz. *Mar. Geol.* 349, 136–151.
- Vandorpe, T., Martins, I., Vitorino, J., Hebbeln, D., García, M., Van Rooij, D., 2016. Bottom currents and their influence on the sedimentation pattern in the El Arraiche mud volcano province, southern Gulf of Cadiz. *Marine Geology* 378, 114–126.
- Veevers, J., 2012. Reconstructions before rifting and drifting reveal the geological connections between Antarctica and its conjugates in Gondwanaland. *Earth Sci. Rev.* 111, 249–318.
- Viana, A., Faugères, J.-C., Stow, D., 1998. Bottom-current-controlled sand deposits—a review of modern shallow-to deep-water environments. *Sediment. Geol.* 115, 53–80.
- Vormann, M., Franke, D., Jokat, W., 2020. The crustal structure of the southern Davie Ridge offshore northern Mozambique – A wide-angle seismic and potential field study. *Tectonophysics* 778, 228370. https://doi.org/10.1016/j.tecto.2020.228370.
- Walford, H., White, N., Sydow, J., 2005. Solid sediment load history of the Zambezi Delta. *Earth Planet. Sci. Lett.* 238, 49–63.
- Wang, X., Zhuo, H., Wang, Y., Mao, P., He, M., Chen, W., Zhou, J., Gao, S., Wang, M., 2018. Controls of contour currents on intra-canyon mixed sedimentary processes: Insights from the Pearl River Canyon, northern South China Sea. *Mar. Geol.* 406, 193–213.
- Wignall, P.B., Bond, D.P.G., 2008. The end-Triassic and Early Jurassic mass extinction records in the British Isles. *Proc. Geol. Assoc.* 119 (1), 73–84.
- Wildeboer Schut, E., Uenzelmann-Neben, G., Gersonde, R., 2002. Seismic evidence for bottom current activity at the Agulhas Ridge. *Glob. Planet. Chang.* 34, 185–198.
- Wiles, E., Green, A., Watkeys, M., Jokat, W., Krockner, R., 2014. A new pathway for Deep water exchange between the Natal Valley and Mozambique Basin? *Geo-Mar. Lett.* 34, 525–540.
- Wiles, E., Green, A., Watkeys, M., Jokat, W., 2017a. The Zambezi Channel: a new perspective on submarine channel evolution at low latitudes. *Geomorphology* 286, 121–132.
- Wiles, E., Green, A., Watkeys, M., Jokat, W., 2017b. Zambezi continental margin: compartmentalized sediment transfer routes to the abyssal Mozambique Channel. *Mar. Geophys. Res.* 38, 227–240.
- Wise Jr., S.W., Breza, J., Harwood, D., Wei, W., Zachos, J., 1992. Paleogene glacial history of Antarctica in light of Leg 120 drilling results. In: Presented at the Proc. Ocean Drill. Program Sci. Results, pp. 1001–1030. https://doi.org/10.2973/odp.proc.sr.120.205.1992.
- World Ocean Database, 2013. https://www.nodc.noaa.gov/OC5/WOD13/.
- Wynn, R.B., Stow, D.A., 2002. Classification and characterisation of deep-water sediment waves. *Mar. Geol.* 192, 7–22.
- Yin, S., Hernández-Molina, F.J., Zhang, W., Li, J., Wang, L., Ding, Weifeng, Ding, Weiwai, 2019. The influence of oceanographic processes on contourite features: a multi-disciplinary study of the northern South China Sea. *Mar. Geol.* 415, 105967.
- Youssef, M., El-Sorogy, A.S., 2015. Paleocology of benthic foraminifera in coral reefs recorded in the Jurassic Tuwaiq Mountain Formation of the Khashm Al-Qaddiyah area, Central Saudi Arabia. *J. Earth Sci.* 26, 224–235.
- Zachos, J.C., Stott, L.D., Lohmann, K.C., 1994. Evolution of early Cenozoic marine temperatures. *Paleoceanography* 9, 353–387.
- Zachos, J., Pagan, M., Sloan, L., Thomas, E., Billups, K., 2001. Trends, rhythms, and aberrations in global climate 65 Ma to present. *Science* 292, 686–693. https://doi.org/10.1126/science.1059412.
- Zhang, J.-J., Wu, S.-H., Fan, T.-E., Fan, H.-J., Jiang, L., Chen, C., Wu, Q.-Y., Lin, P., 2016. Research on the architecture of submarine-fan lobes in the Niger Delta Basin, offshore West Africa. *J. Palaeogeogr.* 5, 185–204.
- Zhou, W., Gao, X., Wang, Yingmin, Zhuo, H., Zhu, W., Xu, Q., Wang, Yongfeng, 2015. Seismic geomorphology and lithology of the early Miocene Pearl River deepwater fan system in the Pearl River Mouth Basin, northern south China sea. *Mar. Pet. Geol.* 68, 449–469.